

Tuning the photoluminescence properties of SLE- and MRL-active tricarbonylrhenium(I) complexes through minor structural changes of the organic ligand

Alexandre Poirot, Nadine Leygue, Béatrice Delavaux-Nicot, Nathalie Saffon-Merceron, Clémence Allain, Eric Benoist and Suzanne Fery-Forgues

NMR characterization

Figure S1. Carbon numbering for attribution of ^1H and ^{13}C NMR chemical shifts of ligands L1 , L2 and L3	2
Figure S2. ^1H NMR spectrum of complex RePBO-Me1 in CDCl_3	3
Figure S3. ^{13}C NMR spectrum of complex RePBO-Me1 in CDCl_3	4
Figure S4. HSQC and HMBC NMR spectra of complex RePBO-Me1 in CDCl_3	5
Figure S5. ^1H NMR spectrum of complex RePBO-Me2 in CDCl_3	6
Figure S6. ^{13}C NMR spectrum of complex RePBO-Me2 in CDCl_3	7
Figure S7. HSQC and HMBC NMR spectra of complex RePBO-Me2 in CDCl_3	8
Figure S8. ^1H NMR spectrum of complex RePBO-Me3 in CDCl_3	9
Figure S9. ^{13}C NMR spectrum of complex RePBO-Me3 in CDCl_3	10
Figure S10. HSQC and HMBC NMR spectra of complex RePBO-Me3 in CDCl_3	11
Figure S11. Variable temperature ^1H NMR spectra of complex RePBO-Me1 in DMSO-d_6	12
Figure S12. Variable temperature ^1H NMR spectra of complex RePBO-Me3 in tetrachloroethane-d2	12

Crystallographic data

Table S1. Selected bond lengths for the methylated complexes and for the parent compound RePBO	13
Table S2. Selected angles ($^\circ$) for the methylated complexes and for the parent compound RePBO	14
Figure S13. Molecular arrangement of pure complex RePBO-Me2 (crystals 2a)	15
Figure S14. Molecular arrangement of the dichloromethane solvate of complex RePBO-Me2 (crystals 2b)	15
Figure S15. Molecular arrangement of the methanol solvate of complex RePBO-Me3	15
Figure S16. Molecular views of the two isomers present in the unit cell of complex RePBO-Me1	16

Quantum chemistry calculations

Table S3. Composition (%) of the frontier molecular orbitals involved in the main electronic transitions of complex RePBO-Me1 in CH_2Cl_2	16
Table S4. Main electronic transitions for RePBO-Me1 in CH_2Cl_2 calculated using TD-DFT	17
Table S5. Composition (%) of the frontier molecular orbitals involved in the main electronic transitions of complex RePBO-Me2 in CH_2Cl_2	17
Table S6. Main electronic transitions for complex RePBO-Me2 in CH_2Cl_2 calculated using TD-DFT	17
Table S7. Composition (%) of the frontier molecular orbitals involved in the main electronic transitions of complex RePBO-Me3 in CH_2Cl_2	18
Table S8. Main electronic transitions for complex RePBO-Me3 in CH_2Cl_2 calculated using TD-DFT	18
Table S9. Comparison of the composition (%) of the first two lowest unoccupied molecular orbitals of the three methylated complexes in CH_2Cl_2	19
Figure S17. Energy levels and isodensity plots of the first frontier molecular orbitals of RePBO-Me1	19
Figure S18. Energy levels and isodensity plots of the first frontier molecular orbitals of RePBO-Me2	20
Figure S19. Energy levels and isodensity plots of the first frontier molecular orbitals of RePBO-Me3	21
Figure S20. Theoretical UV-vis absorption spectra and main electronic transitions for the three methylated complexes in CH_2Cl_2 calculated using the TD-DFT method	21
Figure S21. Representation of the complexes in the lowest MLCT triplet excited state, calculated by DFT. Spin density distribution, position of unpaired electrons in the hole and in the particle	22
Figure S22. Representation of the complexes in the lowest ILCT triplet excited state, calculated by DFT. Spin density distribution, position of unpaired electrons in the hole and in the particle	22
Figure S23. Geometry of the three methylated complexes in the ground state and in the first two excited triplet states $^3\text{ILCT}$ and $^3\text{MLCT}$, calculated by DFT	23
Table S10. Comparison between the phenyl-pyta angle values determined by crystallography and calculated by DFT for molecules in the ground state and in the two lowest-energy triplet states	23

Electrochemistry

Table S11. Selected electrochemical data of the three complexes	24
--	----

Table S12. Experimental electrochemical data and calculated energy gaps (E_g).....	24
Figure S24. Cyclic voltammograms of RePBO-Me1 and of its first oxidation and reduction processes	25
Figure S25. Cyclic voltammograms of the reduction processes of RePBO-Me1	25
Figure S26. Cyclic voltammograms of the first oxidation process of RePBO-Me1	25
Figure S27. Cyclic voltammograms of RePBO-Me2 , and of its first oxidation and reduction processes.....	26
Figure S28. Cyclic voltammograms of the reduction processes of RePBO-Me2	26
Figure S29. Cyclic voltammograms of the first oxidation process of RePBO-Me2	26
Figure S30. Cyclic voltammograms of RePBO-Me3 , and of its first oxidation and reduction processes	27
Figure S31. Cyclic voltammograms of the reduction processes of RePBO-Me3	27
Figure S32. Cyclic voltammograms of the first oxidation process of RePBO-Me3	27

Spectroscopy

Figure S33. Photoluminescence decay of RePBO-Me1 in dichloromethane	28
Figure S34. Photoluminescence decay of RePBO-Me2 in dichloromethane	28
Figure S35. Photoluminescence decay of RePBO-Me3 in dichloromethane	29
Figure S36. AIE behavior of RePBO	29
Figure S37. Fluorescence microscopy images of the complexes as pristine powders and after grinding	30
Figure S38. PLExcitation and emission spectra of RePBO-Me1 as pristine and ground powders	30
Figure S39. PLExcitation and emission spectra of RePBO-Me1 as pristine and ground powders	30
Figure S40. PLExcitation and emission spectra of RePBO-Me1 as pristine and ground powders	31
Figure S41. Photoluminescence decay of RePBO-Me1 as pristine powder	31
Figure S42. Photoluminescence decay of RePBO-Me2 as pristine powder	31
Figure S43. Photoluminescence decay of RePBO-Me3 as pristine powder	32
Figure S44. Photoluminescence decay of RePBO-Me1 as ground powder	32
Figure S45. Photoluminescence decay of RePBO-Me2 as ground powder	32
Figure S46. Photoluminescence decay of RePBO-Me3 as ground powder	33

NMR characterization

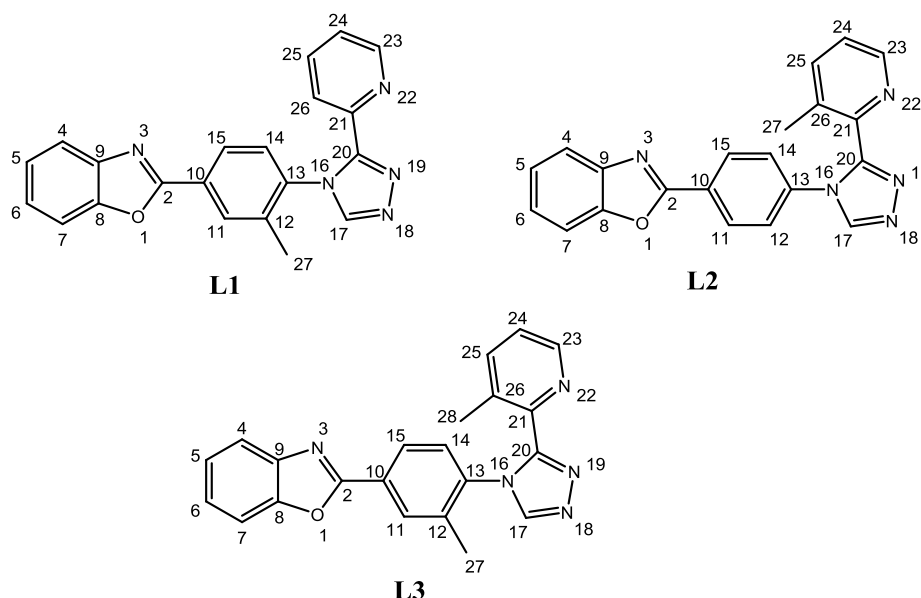


Figure S1. Carbon numbering for attribution of ^1H and ^{13}C NMR chemical shifts of ligands **L1**, **L2** and **L3**.

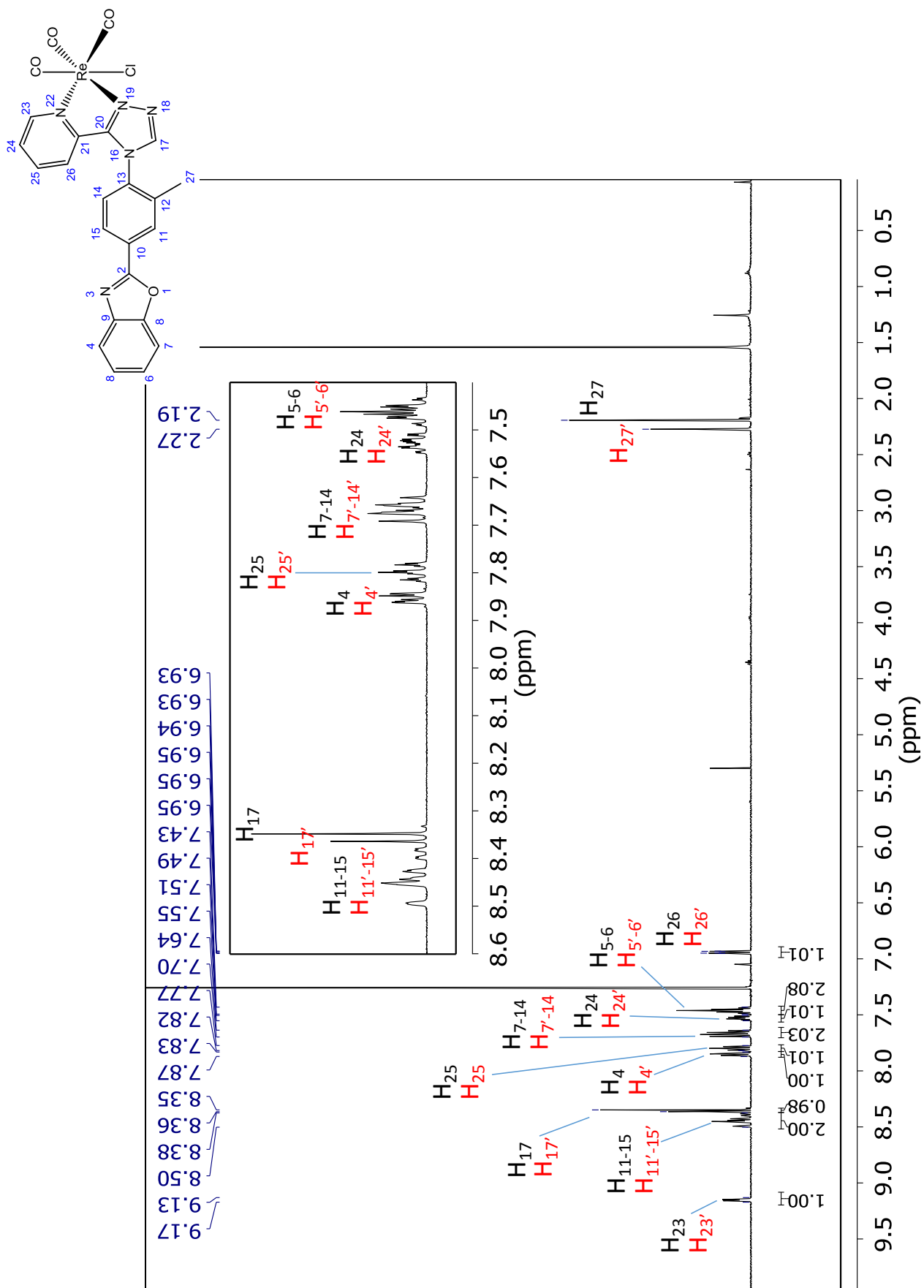


Figure S2. ^1H NMR spectrum of complex **RePBO-Me1** in CDCl_3 at 25°C (500 MHz).

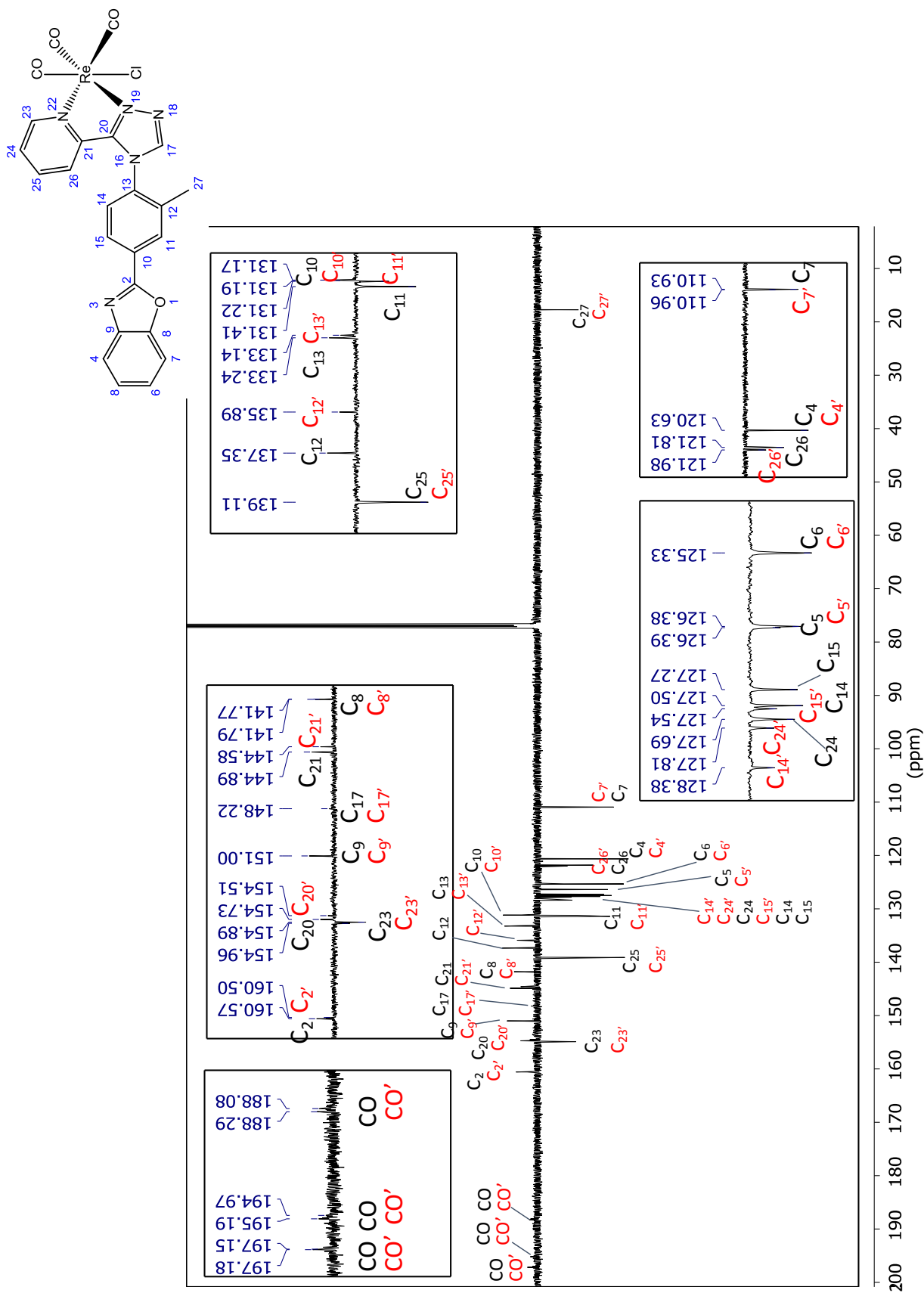


Figure S3. ^{13}C NMR spectrum of complex **RePBO-Me1** in CDCl_3 at 25°C (125 MHz).

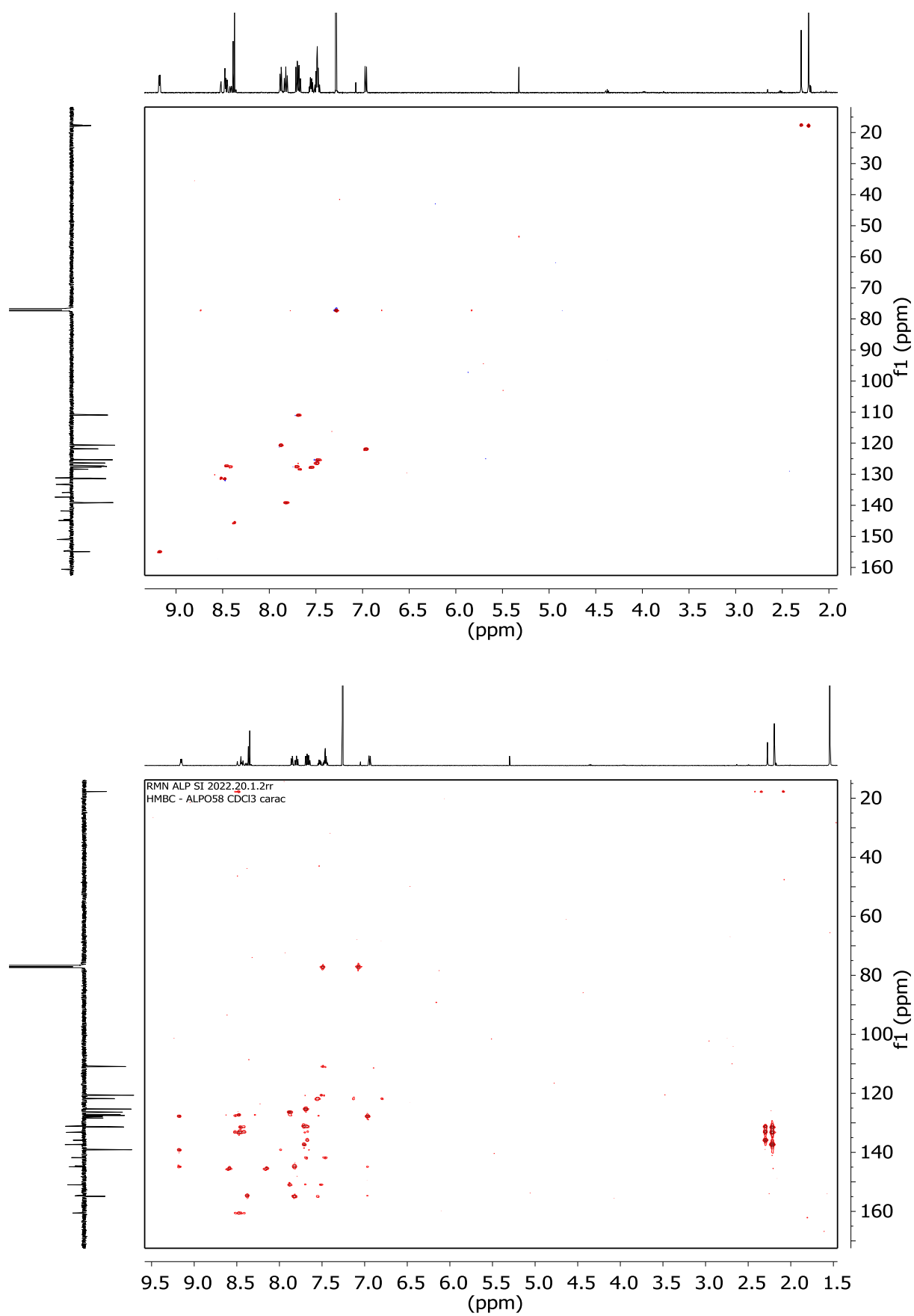


Figure S4. HSQC (top) and HMBC (bottom) NMR spectra of complex **RePBO-Me1** in CDCl_3 at 25° .

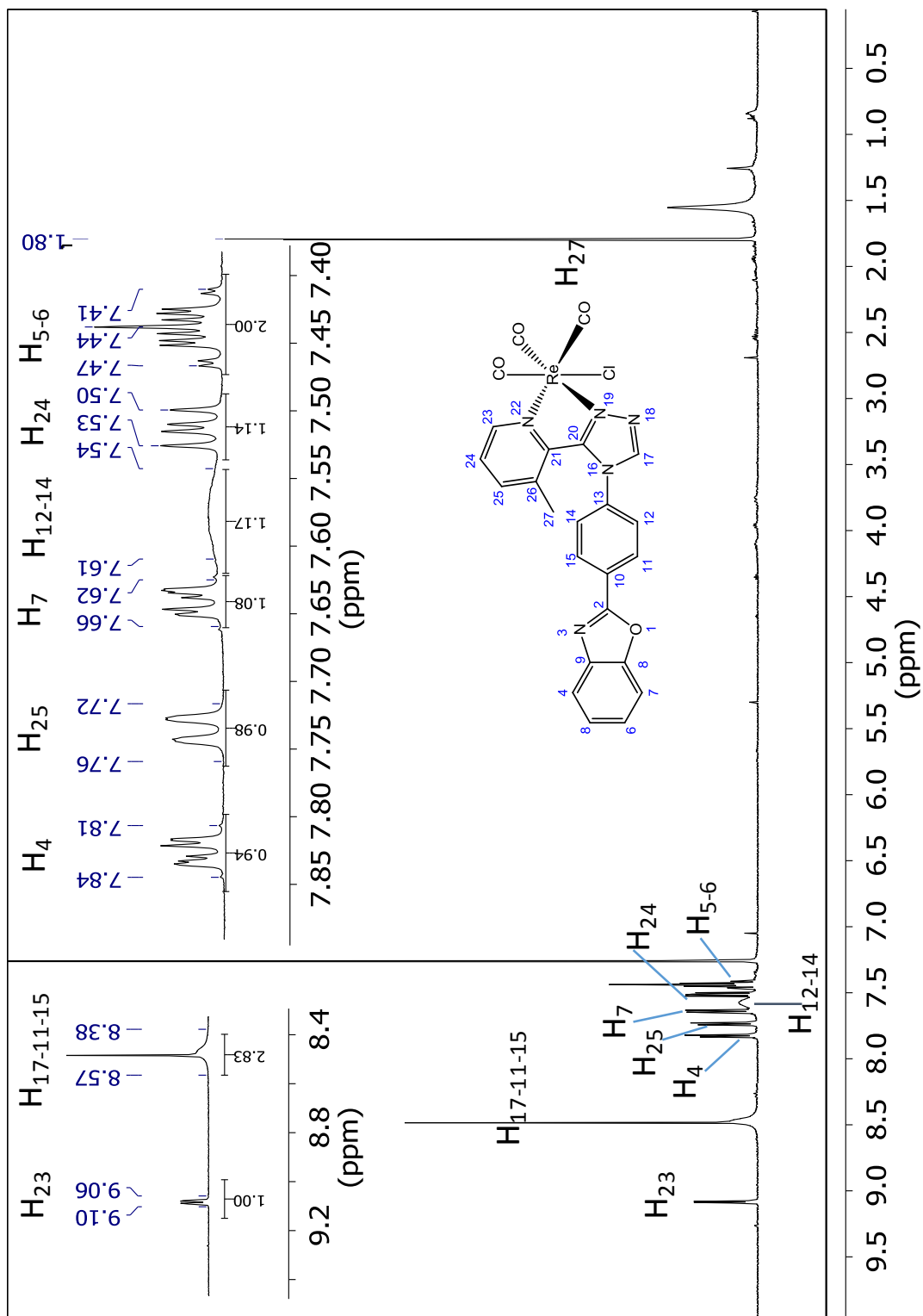


Figure S5. ^1H NMR spectrum of complex **RePBO-Me2** in CDCl_3 at 25°C (500 MHz).

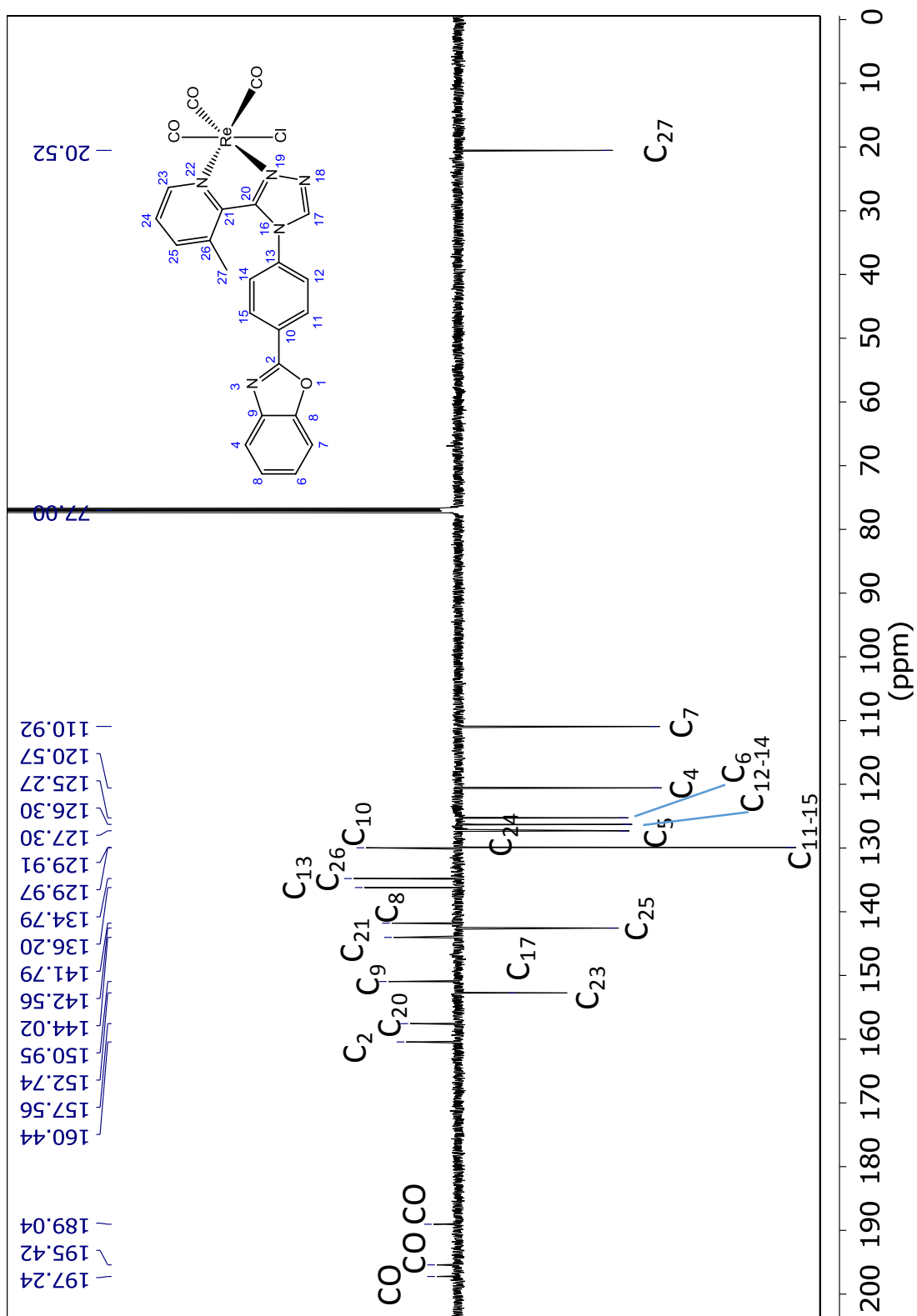


Figure S6. ^{13}C NMR spectrum of complex **RePBO-Me₂** in CDCl_3 at 25°C (125 MHz).

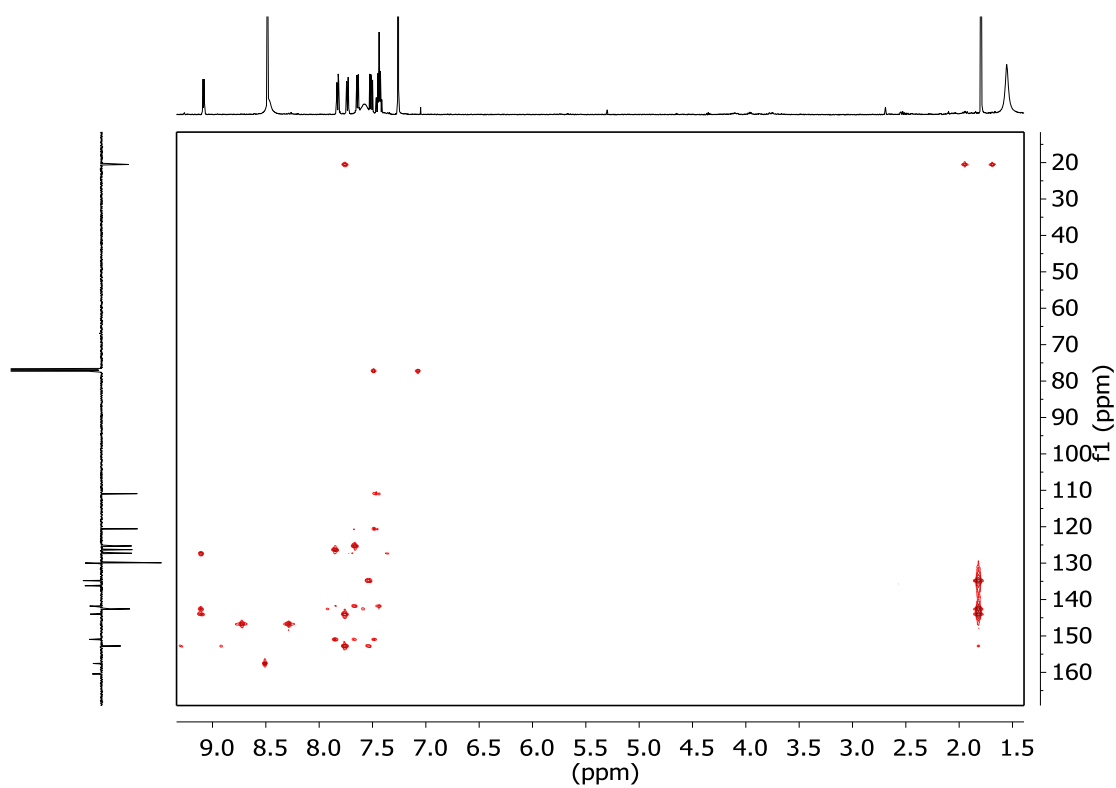
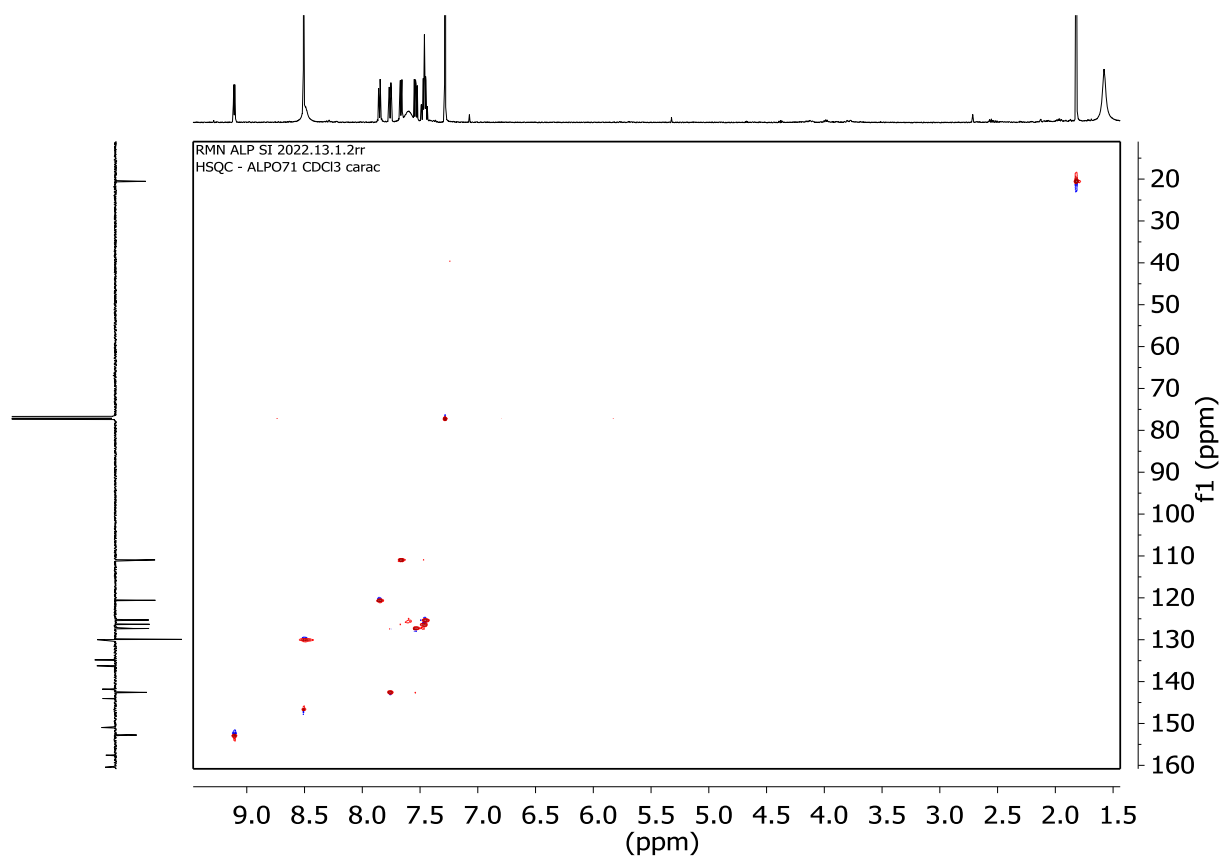


Figure S7. HSQC (top) and HMBC (bottom) NMR spectra of complex **RePBO-Me2** in CDCl_3 at 25° .

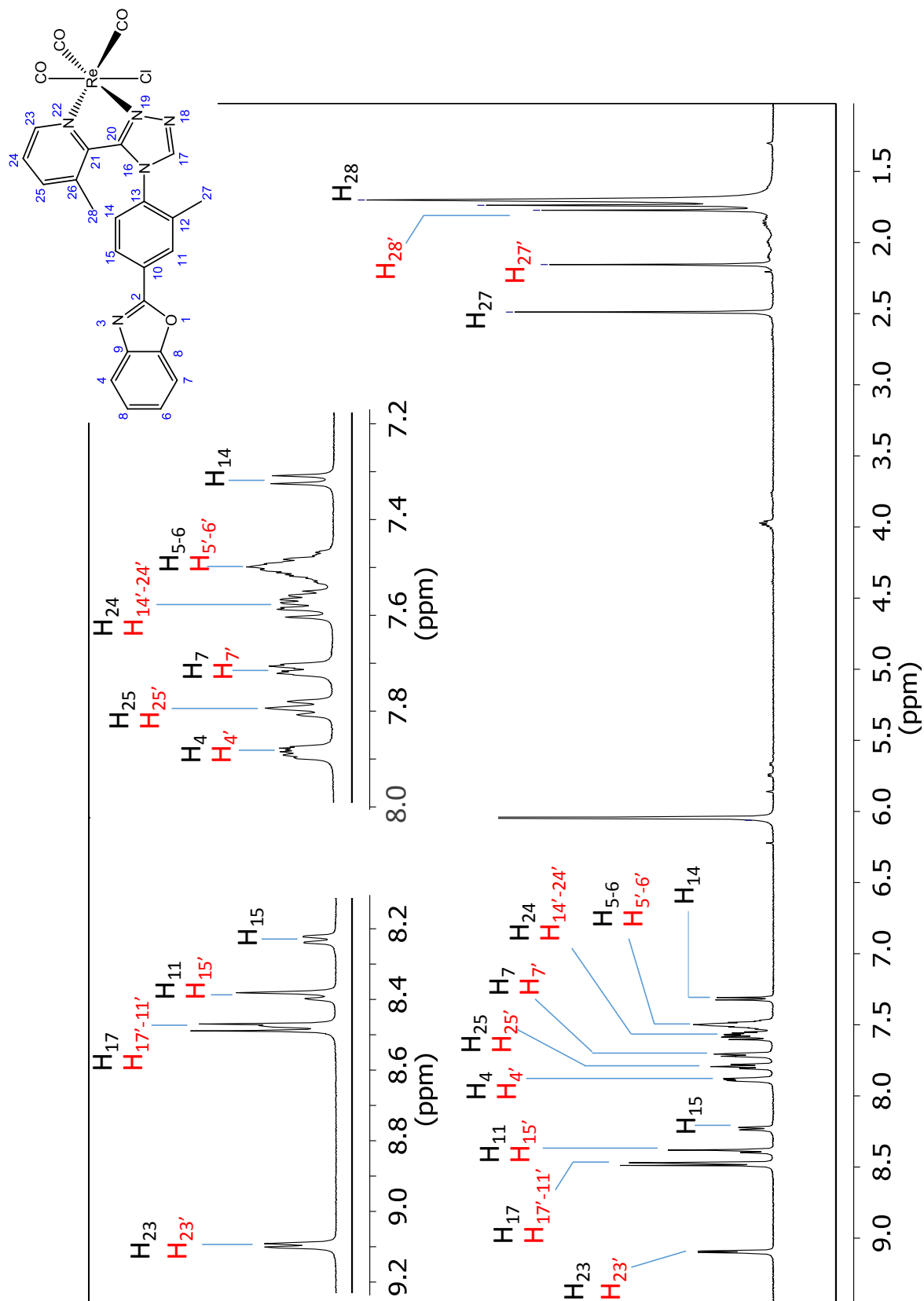


Figure S8. ^1H NMR spectrum of complex **RePBO-Me₃** in tetrachloroethane- d_2 at 25°C (500 MHz).

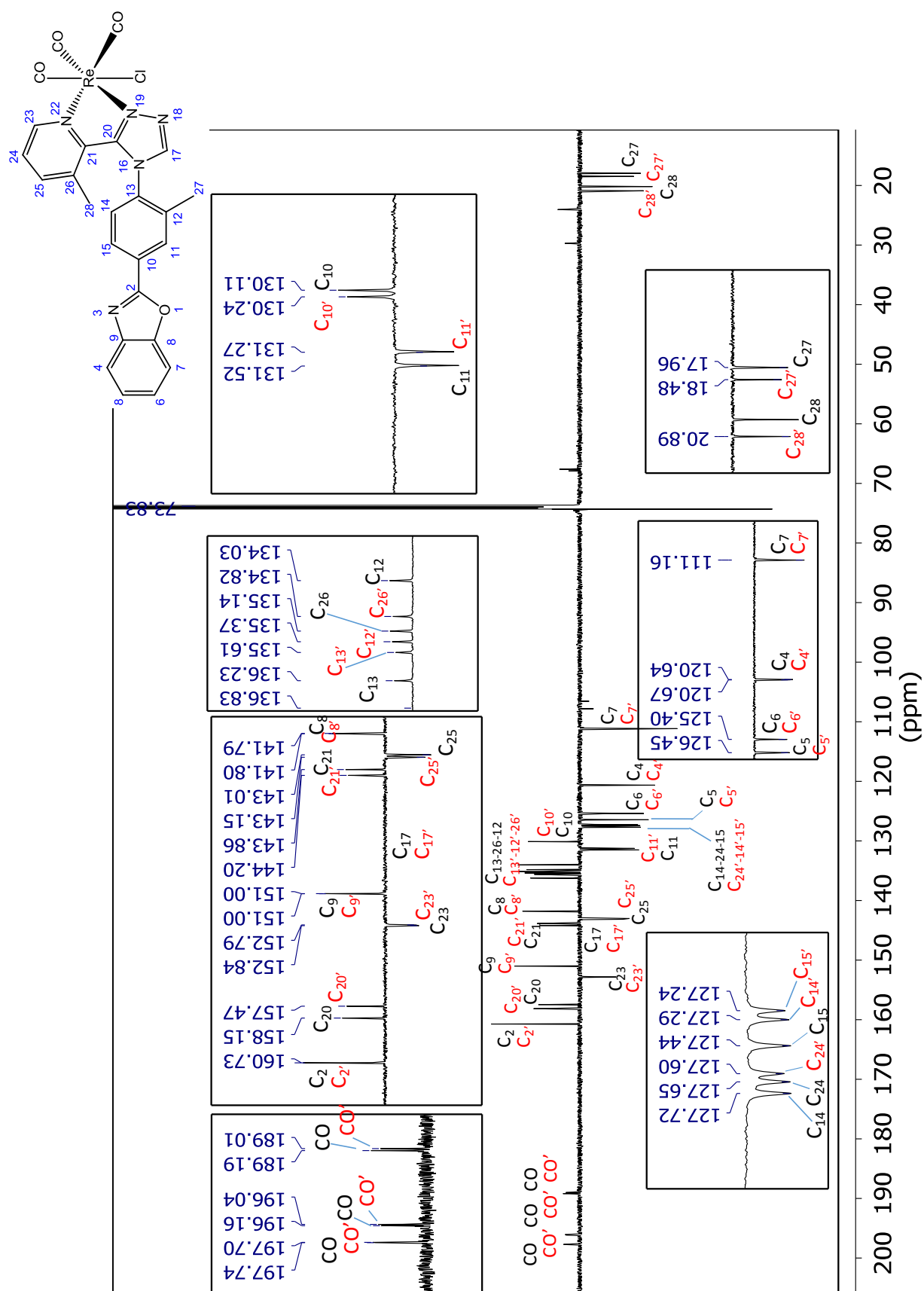


Figure S9. ^{13}C NMR spectrum of complex **RePBO-Me₃** in $\text{tetrachloroethane-}d_2$ at 25°C (125 MHz).

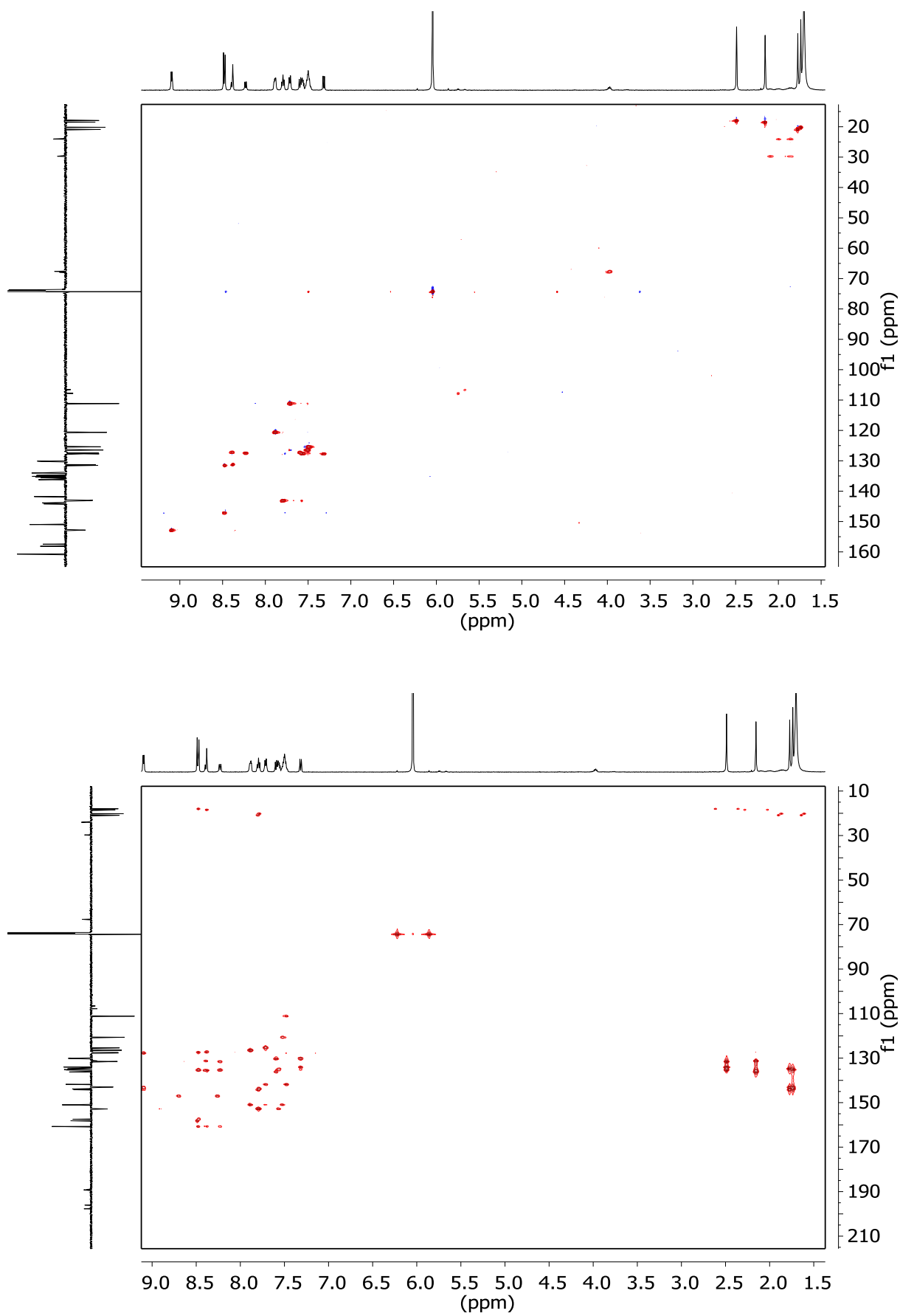


Figure S10. HSQC (top) and HMBC (bottom) NMR spectra of complex **RePBO-Me3** in tetrachloroethane- d_2 at 25° .

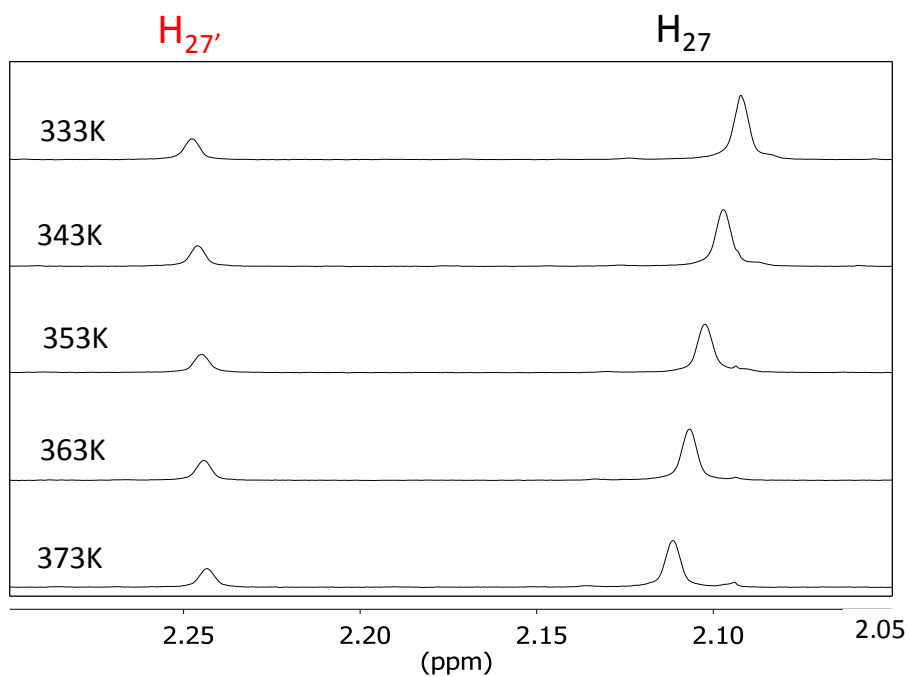


Figure S11. Variable temperature ^1H NMR spectra of complex **RePBO-Me1** in DMSO-d_6 in the region 2.30-2.05 ppm (400 MHz).

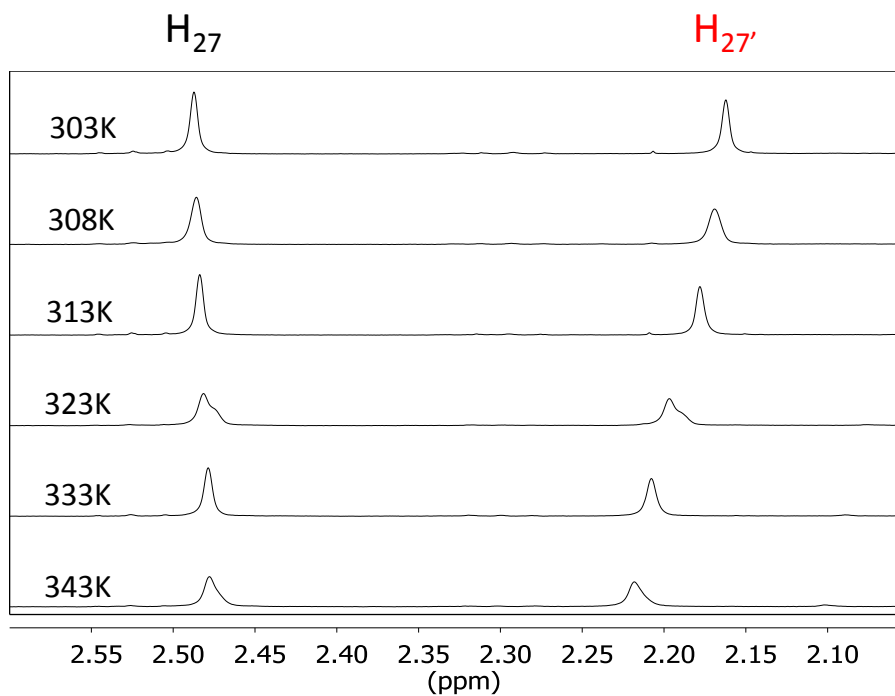
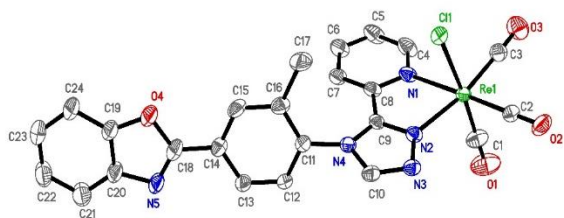


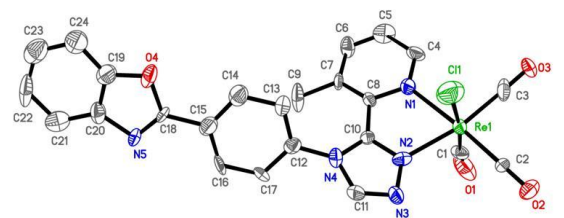
Figure S12. Variable temperature ^1H NMR spectra of complex **RePBO-Me3** in $\text{tetrachloroethane-d}_2$ in the region 2.55-2.10 ppm (400 MHz).

Crystallographic data

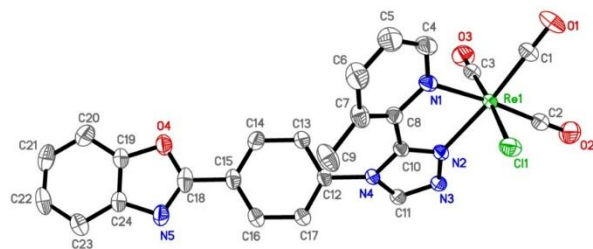
Table S1. Selected bond lengths (Å) for methylated complexes and for the parent compound **RePBO**. Species **RePBO-Me2(a)** and **RePBO-Me2(b)** are the pure form and the dichloromethane solvate of **RePBO-Me2**, respectively. The atoms were numbered like on the molecular views. For the sake of comparison, each line corresponds to the same bond in every complex. For molecular views, the displacement ellipsoids are drawn at the 50% probability level.



RePBO-Me1



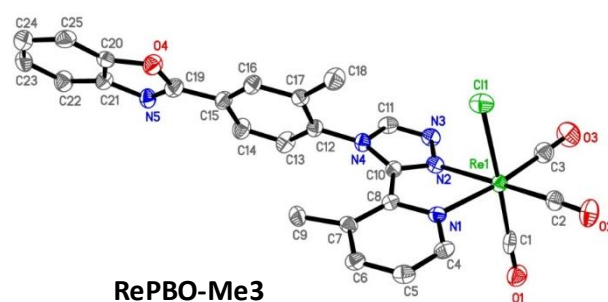
RePBO-Me2(a)



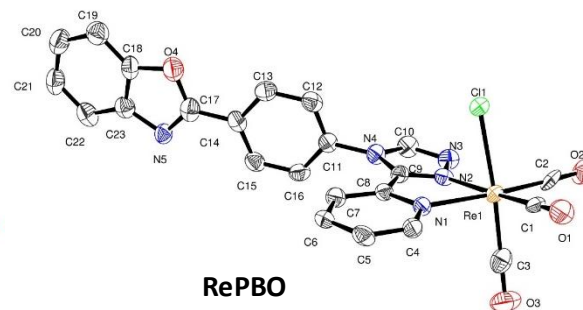
RePBO-Me2(b)

Bond	RePBO-Me1	RePBO-Me2(a)	Bond	RePBO-Me2(b)	RePBO ^a	Bond	RePBO-Me3
Re1-C11	2.474(8)	2.437(6)	Re1-C11	2.480(6)	2.488(2)	Re1-C11	2.482(1)
Re1-N1	2.197(3)	2.227(1)	Re1-N1	2.202(2)	2.198(4)	Re1-N1	2.195(4)
Re1-N2	2.149(3)	2.171(1)	Re1-N2	2.160(2)	2.155(5)	Re1-N2	2.130(4)
Re1-C3	1.927(4)	1.906(2)	Re1-C1	1.918(3)	1.902(7)	Re1-C2	1.914(5)
Re1-C2	1.920(4)	1.903(1)	Re1-C2	1.908(3)	1.920(7)	Re1-C3	1.924(6)
Re1-C1	1.917(4)	1.962(2)	Re1-C3	1.910(3)	1.903(8)	Re1-C1	1.913(6)
O3-C3	1.136(5)	1.136(2)	O1-C1	1.144(3)	1.160(7)	O2-C2	1.154(6)
O2-C2	1.148(4)	1.133(2)	O2-C2	1.156(4)	1.148(7)	O3-C3	1.148(6)
O1-C1	1.128(5)	1.049(2)	O3-C3	1.149(3)	1.151(8)	O1-C1	1.132(6)

^a Data from Wang et al., *Dalton Trans.* **2019**, 48, 15906–15916.



RePBO-Me3



RePBO

Table S2. Selected angles (°) for methylated complexes and for the parent compound **RePBO**. Species **RePBO-Me2(a)** and **RePBO-Me2(b)** are the pure form and the dichloromethane solvate of **RePBO-Me2**, respectively. The atoms were numbered like on the molecular views. The atoms were numbered like on the molecular views. For the sake of comparison, each line corresponds to the same bond in each complex.

Angle	RePBO-Me1	RePBO-Me2(a)	Angle	RePBO-Me2(b)	RePBO ^a	Angle	RePBO-Me3
C2-Re1-C1	89.5(2)	91.0(7)	C2-Re1-C3	87.5(1)	91.0(3)	C3-Re1-C1	89.6(2)
C3-Re1-C1	90.1(2)	93.8(7)	C1-Re1-C3	91.9(1)	87.2(3)	C2-Re1-C1	88.6(2)
C3-Re1-C2	88.9(2)	87.5(6)	C1-Re1-C2	88.0(1)	89.7(2)	C2-Re1-C3	88.5(2)
C1-Re1-N2	94.6(2)	91.5(6)	C3-Re1-N2	92.7(1)	98.4(2)	C1-Re1-N2	96.9(1)
C2-Re1-N2	100.2(2)	101.7(5)	C2-Re1-N2	101.9(1)	97.5(2)	C3-Re1-N2	99.4(2)
C3-Re1-N2	169.8(1)	169.4(6)	C1-Re1-N2	169.3(1)	170.8(2)	C2-Re1-N2	170.4(2)
C1-Re1-N1	95.5(2)	91.3(6)	C3-Re1-N1	96.0(1)	90.9(3)	C1-Re1-N1	92.8(2)
C2-Re1-N1	172.6(1)	174.5(5)	C2-Re1-N1	174.8(1)	172.0(2)	C3-Re1-N1	172.0(2)
C3-Re1-N1	96.7(1)	97.3(6)	C1-Re1-N1	95.7(1)	98.2(2)	C2-Re1-N1	99.1(2)
N2-Re1-N1	73.9(1)	73.3(4)	N2-Re1-N1	74.2(1)	74.5(2)	N2-Re1-N1	72.8(2)
C1-Re1-Cl1	175.7(1)	173.5(5)	C3-Re1-Cl1	176.0(1)	175.0(2)	C1-Re1-Cl1	178.0(2)
C2-Re1-Cl1	92.3(1)	92.8(5)	C2-Re1-Cl1	94.4(1)	94.1(2)	C3-Re1-Cl1	91.9(2)
C3-Re1-Cl1	93.9(1)	91.6(5)	C1-Re1-Cl1	91.6(1)	92.6(2)	C2-Re1-Cl1	92.8(2)
N2-Re1-Cl1	81.2(1)	82.6(3)	N2-Re1-Cl1	83.6(1)	81.2(1)	N2-Re1-Cl1	81.6(1)
N1-Re1-Cl1	82.5(1)	84.5(3)	N1-Re1-Cl1	81.8(1)	84.2(1)	N1-Re1-Cl1	85.5(1)
O3-C3-Re1	178.5(4)	177.9(1)	O1-C1-Re1	177.2(3)	179.4(6)	O2-C2-Re1	177.4(5)
O2-C2-Re1	179.3(3)	174.4(1)	O2-C2-Re1	177.8(3)	178.9(6)	O3-C3-Re1	178.2(5)
O1-C1-Re1	177.5(4)	170.1(2)	O3-C3-Re1	177.4(2)	175.8(6)	O1-C1-Re1	178.1(5)

^a Data from Wang et al., *Dalton Trans.* **2019**, 48, 15906–15916.

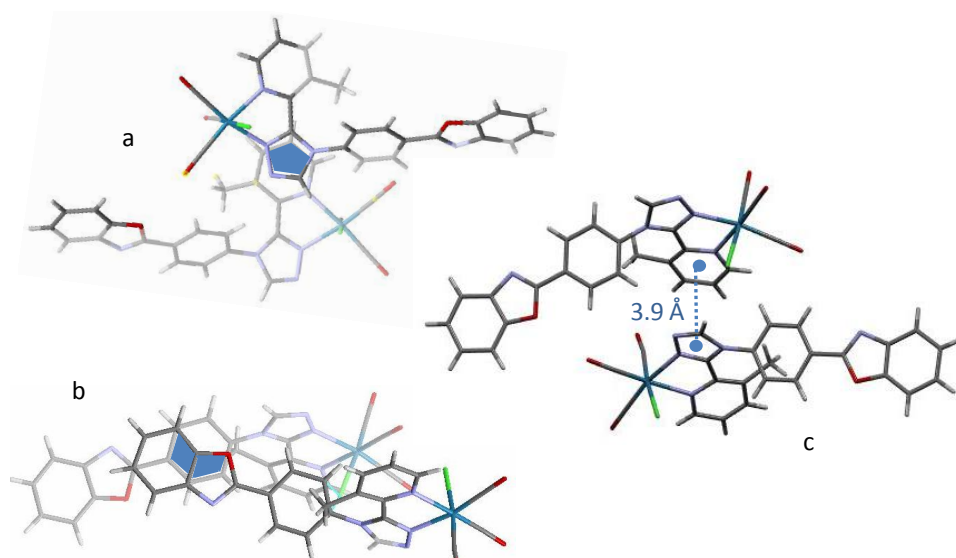


Figure S13. Molecular arrangement of complex **RePBO-Me2(a)**, showing the overlap of aromatic moieties (view perpendicular to the plane of the ring considered) as blue surfaces (a and b) and centroid-to-centroid short contact between the pyridyl and triazole rings (c).

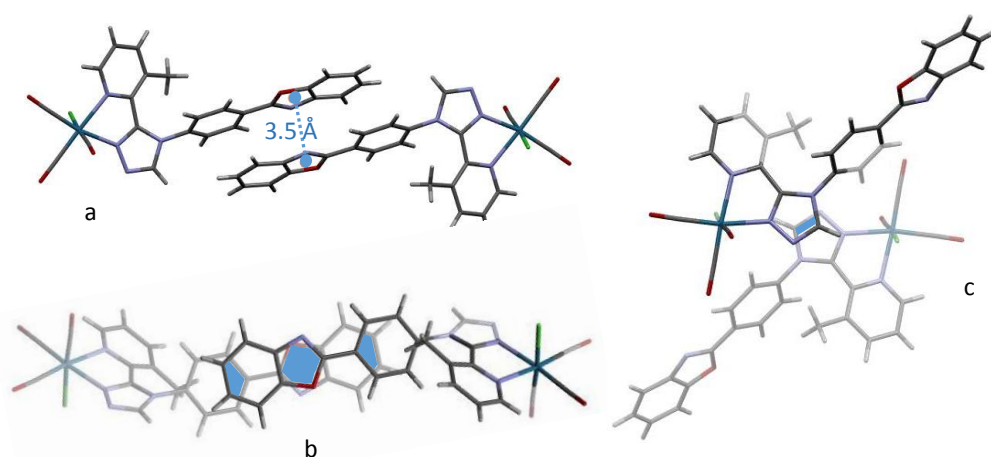


Figure S14. Molecular arrangement of the dichloromethane solvate of complex **RePBO-Me2(b)**, showing the centroid-to-centroid short contact between benzoxazole moieties (a) and the corresponding overlap of aromatic moieties (view perpendicular to the plane of the rings considered) as blue surfaces (b), as well as the very small overlap (blue surface) between triazole groups (c).

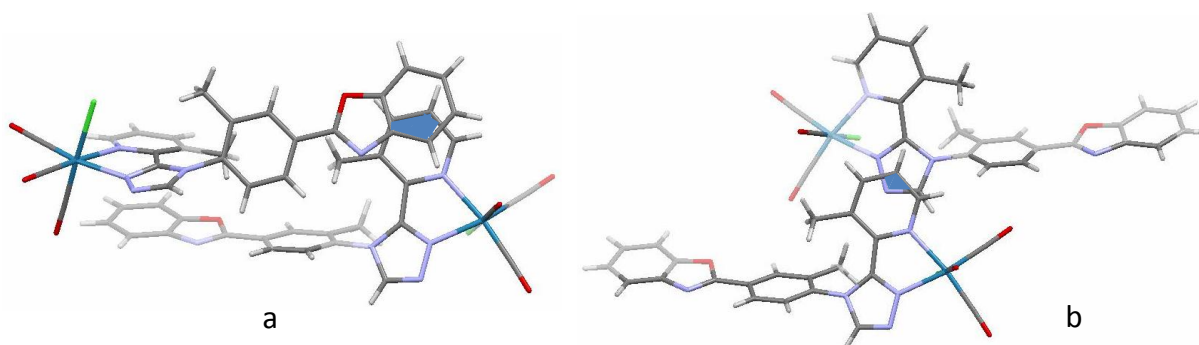


Figure S15. Molecular arrangement of the methanol solvate of complex **RePBO-Me3**, showing the

overlap of the benzoxazole and pyridyl rings (a) and triazole and pyridyl rings (b) as blue surfaces. View perpendicular to the plane of the rings considered.

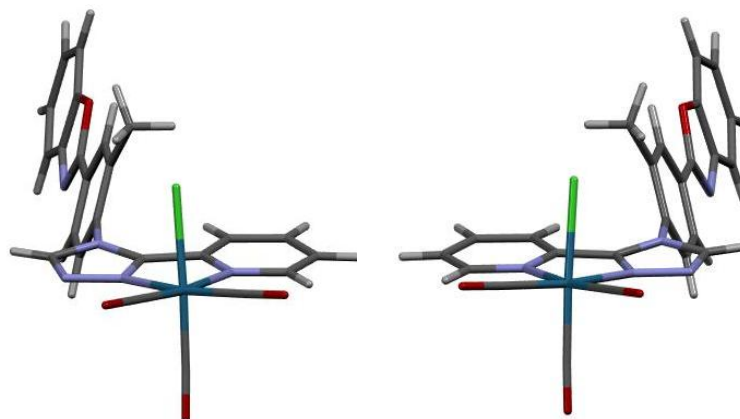


Figure S16. Molecular views of the two enantiomers present in the unit cell of complex **RePBO-Me1**.

Quantum chemistry calculations

Table S3. Composition (%) of the frontier molecular orbitals involved in the main electronic transitions of complex **RePBO-Me1** in CH_2Cl_2 calculated using TD-DFT at the PBE0/LANL2DZ level.

Orbital	Rhenium	Cl	Pyta	PBO	CO
HOMO-12	1.070	0.501	82.871	12.792	2.766
HOMO-9	0.267	0.181	10.447	88.699	0.406
HOMO-8	11.909	43.736	38.378	1.300	4.677
HOMO-7	13.036	68.587	13.234	0.453	4.690
HOMO-5	1.612	29.426	67.071	1.406	0.485
HOMO-4	0.001	0.001	0.012	99.985	0.001
HOMO-3	63.936	0.730	2.113	0.892	32.329
HOMO-2	0.789	0.071	1.191	97.541	0.408
HOMO-1	49.550	20.343	5.148	0.234	24.725
HOMO	49.870	19.249	4.548	0.248	26.085
LUMO	2.598	0.956	87.256	5.397	3.793
LUMO+1	0.115	0.037	6.776	92.835	0.236
LUMO+2	0.142	0.110	93.082	5.104	1.562
LUMO+3	0.349	0.024	10.718	88.473	0.436
LUMO+4	33.870	0.776	2.176	0.928	62.250
LUMO+5	26.701	2.808	12.849	3.416	54.226
LUMO+8	0.389	0.023	9.673	89.238	0.677

Table S4. Main electronic transitions of complex **RePBO-Me1** in dichloromethane calculated using TD-DFT at the PBE0/LANL2DZ level. λ : wavelength. E : energy. f : oscillator strength.

Electronic transition	Contribution	Assignment	Character	λ (nm)	E (eV)	f
$S_0 \rightarrow S_3$	H-1 \rightarrow LUMO	$d(\text{Re}) + \pi(\text{CO}) + p(\text{Cl}) + \pi(\text{Pyta}) \rightarrow \pi^*(\text{Pyta}) + \pi^*(\text{PBO})$	MLCT/XLCT	422.3	2.94	0.1119
$S_0 \rightarrow S_8$	H-4 \rightarrow LUMO	$\pi(\text{PBO}) \rightarrow \pi^*(\text{Pyta}) + \pi^*(\text{PBO})$	ILCT	359.1	3.45	0.0431
$S_0 \rightarrow S_{19}$	H-7 \rightarrow LUMO	$p(\text{Cl}) + \pi(\text{Pyta}) + d(\text{Re}) \rightarrow \pi^*(\text{Pyta}) + \pi^*(\text{PBO})$	XLCT/MLCT	294.7	4.21	0.7799
$S_0 \rightarrow S_{22}$	H-2 \rightarrow L+1	$\pi(\text{PBO}) \rightarrow \pi^*(\text{PBO}) + \pi^*(\text{Pyta})$	ILCT	288.3	4.30	0.3969
$S_0 \rightarrow S_{30}$	H-8 \rightarrow LUMO	$p(\text{Cl}) + \pi(\text{Pyta}) + d(\text{Re}) \rightarrow \pi^*(\text{Pyta}) + \pi^*(\text{PBO})$	XLCT/MLCT	254	4.88	0.0955
$S_0 \rightarrow S_{32}$	H-5 \rightarrow L+2	$\pi(\text{Pyta}) + p(\text{Cl}) \rightarrow \pi^*(\text{Pyta})$	XLCT	251.5	4.93	0.0406
$S_0 \rightarrow S_{34}$	H-1 \rightarrow L+8	$d(\text{Re}) + \pi(\text{CO}) + p(\text{Cl}) + \pi(\text{Pyta}) \rightarrow \pi^*(\text{PBO}) + \pi^*(\text{Pyta})$	MLCT/LLCT/ XLCT	251.4	4.93	0.0598
$S_0 \rightarrow S_{44}$	H-7 \rightarrow L+2	$p(\text{Cl}) + \pi(\text{Pyta}) + d(\text{Re}) \rightarrow \pi^*(\text{Pyta}) + \pi^*(\text{PBO})$	XLCT/MLCT	234.1	5.30	0.0720
$S_0 \rightarrow S_{47}$	H-5 \rightarrow L+3	$\pi(\text{Pyta}) + p(\text{Cl}) \rightarrow \pi^*(\text{PBO}) + \pi^*(\text{Pyta})$	LLCT/XLCT	224.3	5.53	0.0317
$S_0 \rightarrow S_{49}$	H-12 \rightarrow L+1	$\pi(\text{PBO}) + \pi(\text{Pyta}) \rightarrow \pi^*(\text{PBO}) + \pi^*(\text{Pyta})$	ILCT	222.8	5.57	0.0634
$S_0 \rightarrow S_{52}$	H-2 \rightarrow L+5	$\pi(\text{PBO}) \rightarrow \pi^*(\text{CO}) + p(\text{Re})$	LLCT/LMCT	221.4	5.60	0.1025
$S_0 \rightarrow S_{54}$	H-12 \rightarrow LUMO	$\pi(\text{Pyta}) + \pi(\text{PBO}) \rightarrow \pi^*(\text{Pyta}) + \pi^*(\text{PBO})$	ILCT	220.6	5.62	0.0488
$S_0 \rightarrow S_{55}$	H-9 \rightarrow L+1	$\pi(\text{PBO}) + \pi(\text{Pyta}) \rightarrow \pi^*(\text{PBO}) + \pi^*(\text{Pyta})$	ILCT	220.2	5.63	0.1247
$S_0 \rightarrow S_{59}$	H-5 \rightarrow L+4	$\pi(\text{Pyta}) + p(\text{Cl}) \rightarrow \pi^*(\text{CO}) + p(\text{Re})$	LLCT/LMCT/ XLCT/XMCT	213.8	5.80	0.0680

Table S5. Composition (%) of the frontier molecular orbitals involved in the main electronic transitions of complex **RePBO-Me2** in CH_2Cl_2 calculated using TD-DFT at the PBE0/LANL2DZ level.

5Re	6Cl	fragment methylpyta	fragment PBO	fragment CO	total
1.14145	20.45836	77.25554	0.85907	0.28558	100.0000
0.0005	0.00077	0.08513	99.91308	0.00052	100.0000
63.69516	1.59618	2.07248	0.32283	32.31336	100.0000
0.88463	0.50952	2.53508	95.64672	0.42406	100.0000
48.6782	19.04267	6.62892	0.98806	24.66216	100.0000
50.56954	18.12834	4.68357	0.90569	25.71285	100.0000
2.63735	0.8282	75.59859	17.61941	3.31645	100.0000
0.45168	0.13168	19.20167	79.51315	0.70181	100.0000
0.15431	0.09265	93.51344	4.61426	1.62534	100.0000
0.05455	0.00598	7.18101	92.56979	0.18867	100.0000
36.92583	1.33009	4.93523	0.40562	56.40323	100.0000
26.96799	2.23646	14.89572	3.13128	52.76854	100.0000

Table S6. Main electronic transitions of complex **RePBO-Me2** in dichloromethane calculated using TD-DFT at the PBE0/LANL2DZ level. λ : wavelength. E : energy. f : oscillator strength.

Electronic transition	Contribution	Assignment	Character	λ (nm)	E (eV)	f
$S_0 \rightarrow S_2$	H-1 \rightarrow LUMO	$d(\text{Re}) + \pi(\text{CO}) + p(\text{Cl}) + \pi(\text{Pyta}) \rightarrow \pi^*(\text{Pyta}) + \pi^*(\text{PBO})$	MLCT/XLCT	423.2	2.93	0.1273
$S_0 \rightarrow S_5$	H-2 \rightarrow LUMO	$\pi(\text{PBO}) \rightarrow \pi^*(\text{Pyta}) + \pi^*(\text{PBO})$	ILCT	388	3.20	0.2502

$S_0 \rightarrow S_8$	H-4→LUMO	$\pi(\text{PBO}) \rightarrow \pi^*(\text{Pyta}) + \pi^*(\text{PBO})$	ILCT	323	3.84	0.1692
$S_0 \rightarrow S_{12}$	H-6→LUMO	$p(\text{Cl}) + \pi(\text{Pyta}) + d(\text{Re}) + \pi(\text{PBO}) \rightarrow \pi^*(\text{Pyta}) + \pi^*(\text{PBO})$	XLCT/MLCT	300.9	4.12	0.1367
$S_0 \rightarrow S_{15}$	H-2→L+1	$\pi(\text{PBO}) \rightarrow \pi^*(\text{PBO}) + \pi^*(\text{Pyta})$	ILCT	289.1	4.29	0.6605
$S_0 \rightarrow S_{24}$	H-7→LUMO	$p(\text{Cl}) + \pi(\text{Pyta}) + d(\text{Re}) \rightarrow \pi^*(\text{Pyta}) + \pi^*(\text{PBO})$	XLCT/MLCT	265.2	4.68	0.0936
$S_0 \rightarrow S_{32}$	H-9→LUMO	$\pi(\text{PBO}) + \pi(\text{Pyta}) + p(\text{Cl}) \rightarrow \pi^*(\text{Pyta}) + \pi^*(\text{PBO})$	ILCT/XLCT	251.5	4.93	0.0572
$S_0 \rightarrow S_{39}$	H-5→L+2	$\pi(\text{Pyta}) + p(\text{Cl}) \rightarrow \pi^*(\text{Pyta})$	XLCT	235.5	5.27	0.0611
$S_0 \rightarrow S_{46}$	H-5→L+3	$\pi(\text{Pyta}) + p(\text{Cl}) \rightarrow \pi^*(\text{PBO}) + \pi^*(\text{Pyta})$	ILCT/XLCT	225.3	5.50	0.0716
$S_0 \rightarrow S_{54}$	H-2→L+4	$\pi(\text{PBO}) \rightarrow \pi^*(\text{CO}) + p(\text{Re})$	LLCT/LMCT	221.7	5.59	0.0418
$S_0 \rightarrow S_{55}$	H-9→L+1	$\pi(\text{PBO}) + \pi(\text{Pyta}) + p(\text{Cl}) \rightarrow \pi^*(\text{PBO}) + \pi^*(\text{Pyta})$	XLCT	220.3	5.63	0.1139

Table S7. Composition (%) of the frontier molecular orbitals involved in the main electronic transitions of complex **RePBO-Me3** in CH_2Cl_2 calculated using TD-DFT at the PBE0/LANL2DZ level.

Orbital	Rhenium	Cl	Pyta	PBO	CO
HOMO-7	11.577	63.505	16.479	4.380	4.059
HOMO-6	1.222	10.681	10.689	76.871	0.537
HOMO-5	0.698	17.400	65.926	15.844	0.132
HOMO-4	0.002	0.020	0.214	99.763	0.001
HOMO-3	63.629	0.862	2.692	0.256	32.561
HOMO-2	0.559	0.232	1.592	97.341	0.275
HOMO-1	48.241	19.565	6.813	0.769	24.611
HOMO	50.300	19.010	4.328	0.250	26.112
LUMO	2.387	0.954	84.725	7.794	4.140
LUMO+1	0.121	0.050	9.205	90.327	0.297
LUMO+2	0.085	0.098	95.580	2.386	1.851
LUMO+3	0.198	0.044	10.301	88.947	0.510
LUMO+4	39.076	0.840	2.955	0.639	56.489
LUMO+5	27.979	2.716	11.689	4.132	53.484

Table S8. Main electronic transitions of complex **RePBO-Me3** in dichloromethane calculated using TD-DFT at the PBE0/LANL2DZ level. λ : wavelength. E : energy. f : oscillator strength.

Electronic transition	Contribution	Assignment	Character	λ (nm)	E (eV)	f
$S_0 \rightarrow S_2$	H-1→LUMO	$d(\text{Re}) + \pi(\text{CO}) + p(\text{Cl}) + \pi(\text{Pyta}) \rightarrow \pi^*(\text{Pyta}) + \pi^*(\text{PBO})$	MLCT/XLCT	419.7	2.95	0.1288
$S_0 \rightarrow S_5$	H-2→LUMO	$\pi(\text{PBO}) \rightarrow \pi^*(\text{Pyta}) + \pi^*(\text{PBO})$	ILCT	400.4	3.10	0.1214
$S_0 \rightarrow S_{12}$	H-4→LUMO	$\pi(\text{PBO}) \rightarrow \pi^*(\text{Pyta}) + \pi^*(\text{PBO})$	ILCT	302.3	4.10	0.4034
$S_0 \rightarrow S_{15}$	H-1→L+2	$d(\text{Re}) + \pi(\text{CO}) + p(\text{Cl}) + \pi(\text{Pyta}) \rightarrow \pi^*(\text{Pyta})$	MLCT/LLCT/ILCT	297	4.18	0.0505
$S_0 \rightarrow S_{17}$	H-2→L+1	$\pi(\text{PBO}) \rightarrow \pi^*(\text{PBO}) + \pi^*(\text{Pyta})$	ILCT	294.5	4.21	0.5933
$S_0 \rightarrow S_{18}$	H-6→LUMO	$\pi(\text{PBO}) + \pi(\text{Pyta}) + p(\text{Cl}) \rightarrow \pi^*(\text{Pyta}) + \pi^*(\text{PBO})$	MLCT	292.6	4.24	0.0883
$S_0 \rightarrow S_{22}$	H-3→L+2	$d(\text{Re}) + \pi(\text{CO}) \rightarrow \pi^*(\text{Pyta})$	MLCT/LLCT	273.6	4.53	0.0576
$S_0 \rightarrow S_{28}$	H-7→LUMO	$p(\text{Cl}) + \pi(\text{Pyta}) + d(\text{Re}) \rightarrow \pi^*(\text{Pyta}) + \pi^*(\text{PBO})$	XLCT/MLCT	260.5	4.76	0.0413
$S_0 \rightarrow S_{42}$	H-5→L+2	$\pi(\text{Pyta}) + p(\text{Cl}) \rightarrow \pi^*(\text{Pyta})$	XLCT	235.8	5.26	0.0622
$S_0 \rightarrow S_{50}$	H-2→L+5	$\pi(\text{PBO}) \rightarrow \pi^*(\text{CO}) + p(\text{Re}) + \pi^*(\text{Pyta})$	LLCT/LMCT/ILCT	222.3	5.58	0.0839
$S_0 \rightarrow S_{53}$	H-4→L+3	$\pi(\text{PBO}) \rightarrow \pi^*(\text{PBO}) + \pi^*(\text{Pyta})$	ILCT	221.3	5.60	0.1376

Table S9. Comparison of the composition (%) of the first two lowest unoccupied molecular orbitals of the methylated complexes in CH₂Cl₂ calculated using TD-DFT at the PBE0/LANL2DZ level.

Orbital	Complex	Rhenium	Cl	Pyta	PBO	CO
LUMO	RePBO-Me 1	2.598	0.956	87.256	5.397	3.793
	RePBO-Me 2	2.638	0.828	75.599	17.619	3.316
	RePBO-Me 3	2.387	0.954	84.725	7.794	4.140
LUMO+1	RePBO-Me 1	0.115	0.037	6.776	92.835	0.236
	RePBO-Me 2	0.452	0.132	19.201	79.513	0.702
	RePBO-Me 3	0.121	0.050	9.205	90.327	0.297

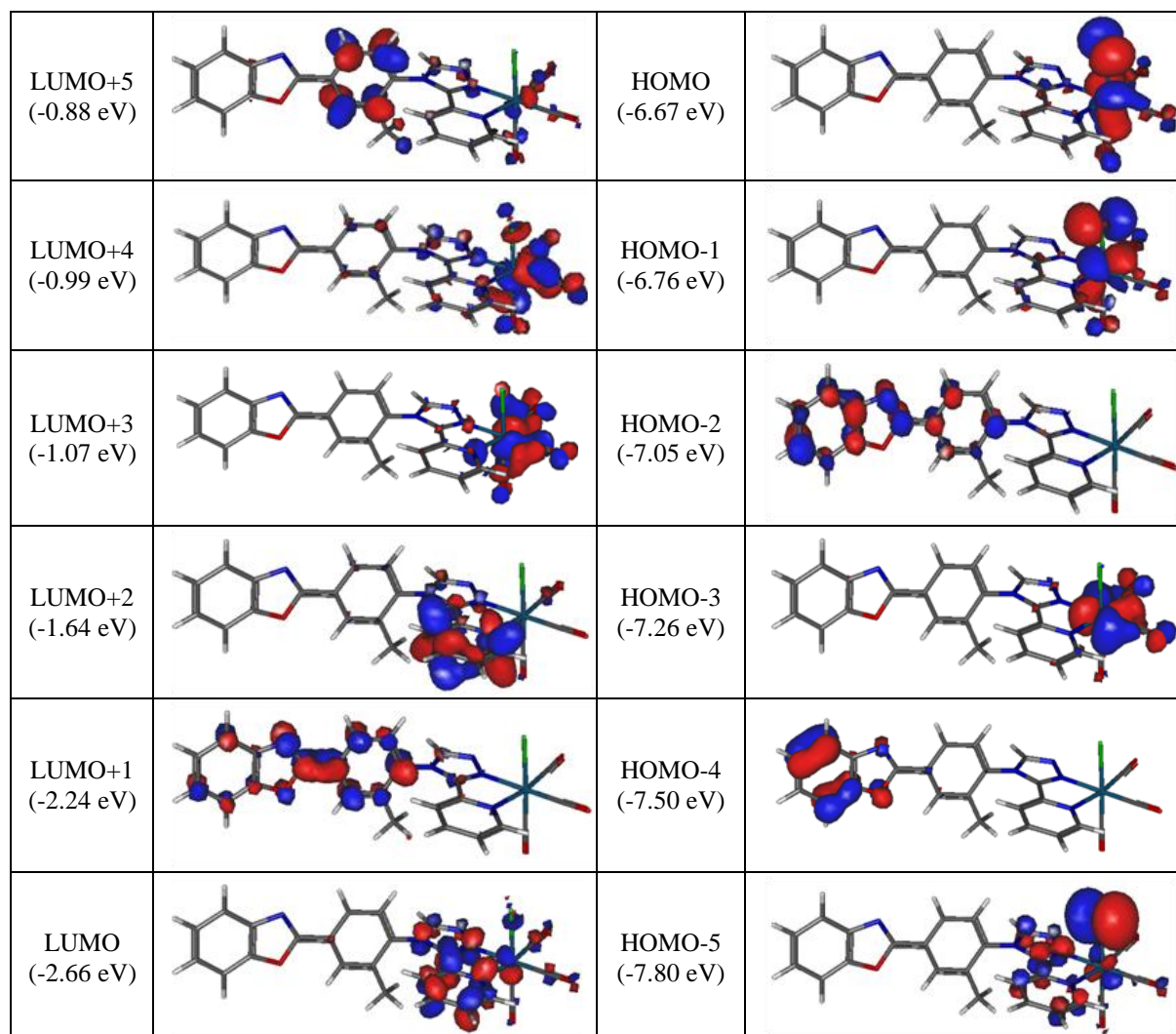


Figure S17. Isodensity plots (isovalue = 0.03 e bohr⁻³) and energy levels of the first frontier molecular orbitals for complex **RePBO-Me1** in dichloromethane calculated by DFT at the PBE0/LANL2DZ level of theory.

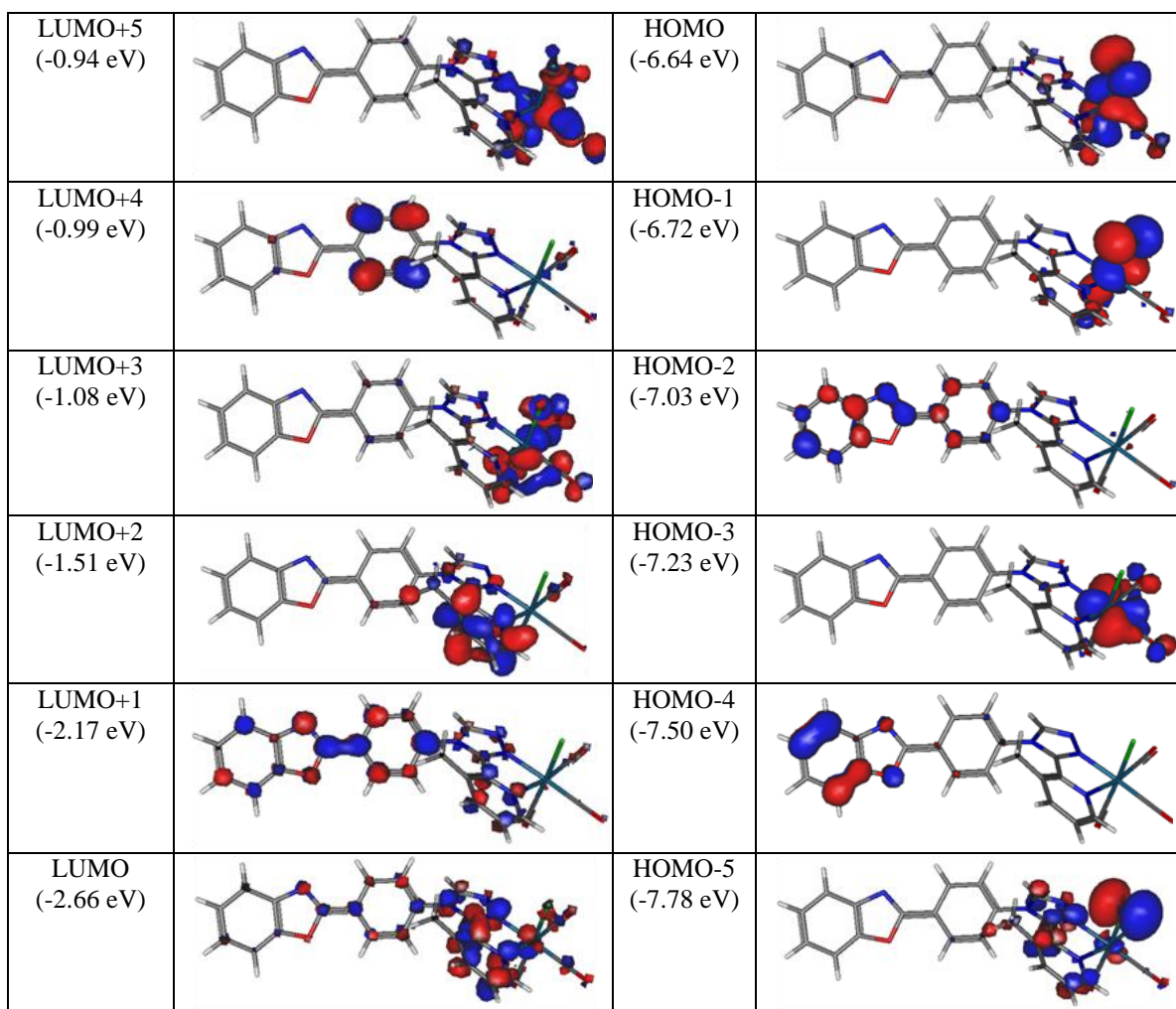
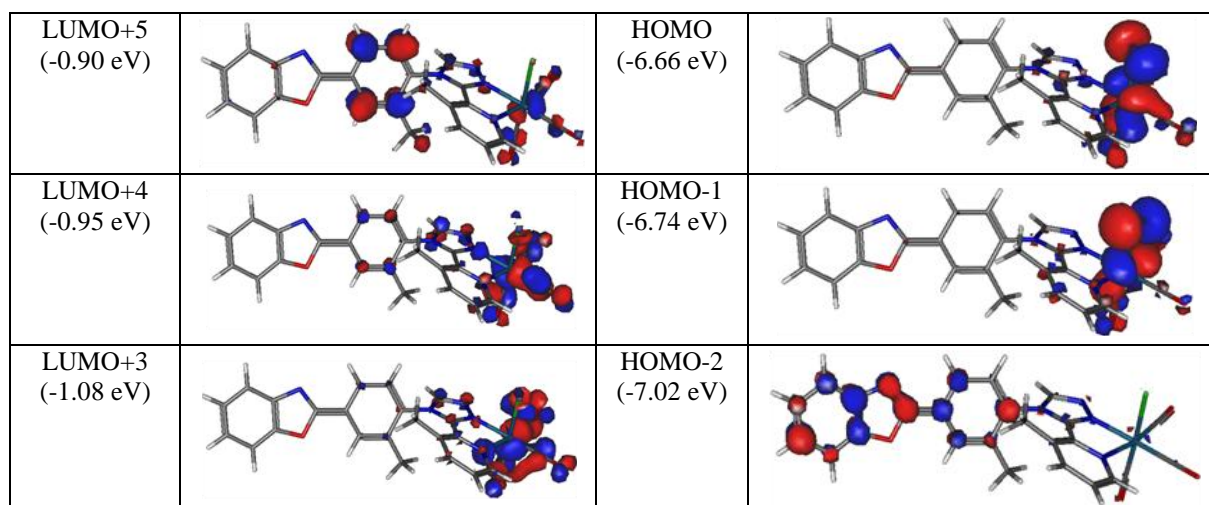


Figure S18. Isodensity plots (isovalue = 0.03 e bohr⁻³) and energy levels of the first frontier molecular orbitals for complex **RePBO-Me2** in dichloromethane calculated by DFT at the PBE0/LANL2DZ level of theory.



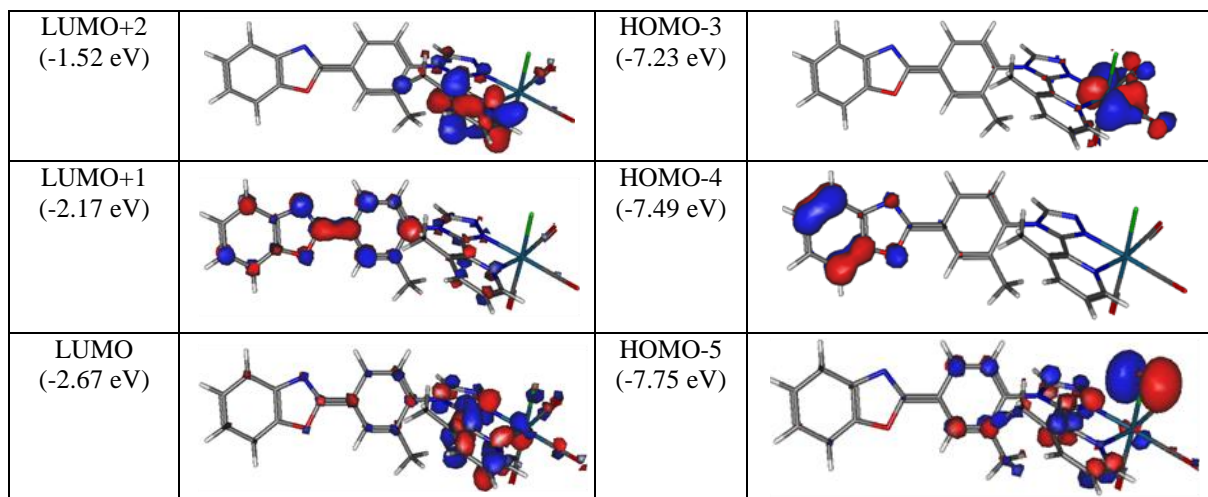


Figure S19. Isodensity plots (isovalue = 0.03 e bohr⁻³) and energy levels of the first frontier molecular orbitals for complex **RePBO-Me3** in dichloromethane calculated by DFT at the PBE0/LANL2DZ level of theory.

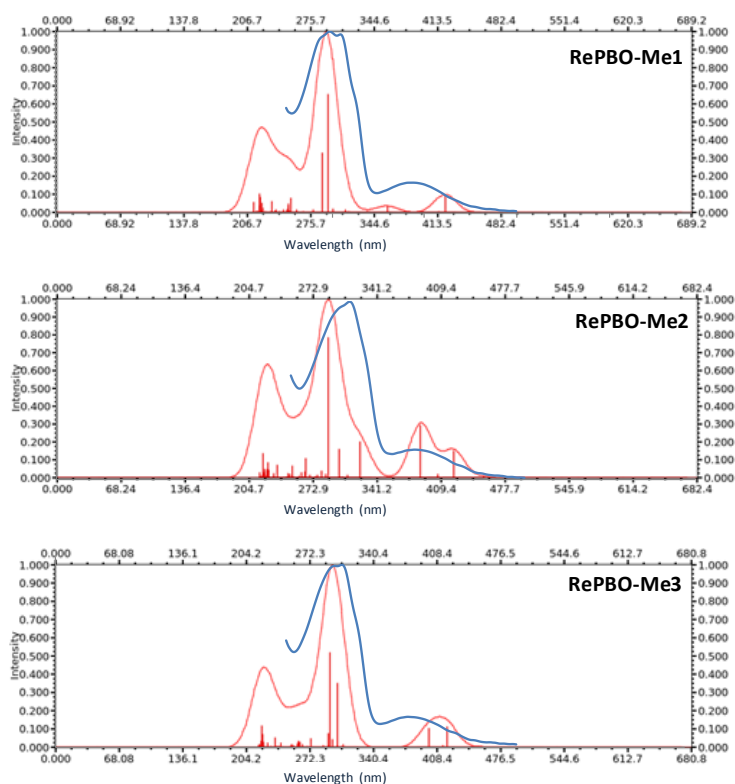


Figure S20. From top to bottom: Theoretical UV-vis absorption spectra and main electronic transitions for complexes **RePBO-Me1**, **RePBO-Me2** and **RePBO-Me3** in CH₂Cl₂ calculated using the TD-DFT method at the PBE0/LANL2DZ level (red lines). Comparison with the experimental spectra (blue lines).

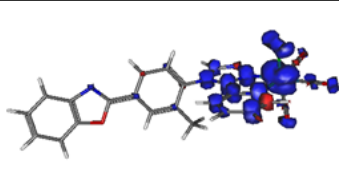

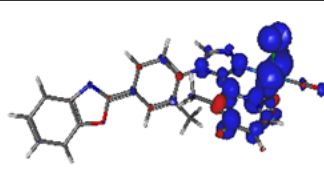
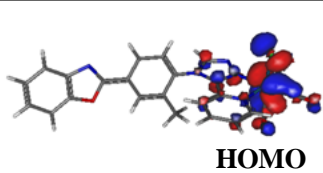
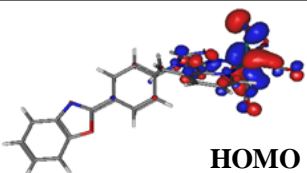
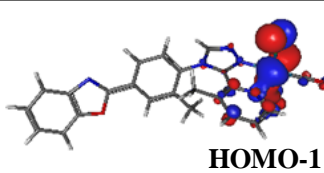
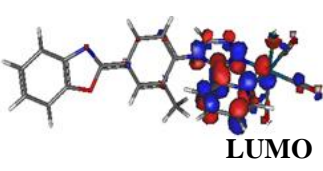
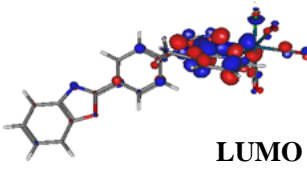
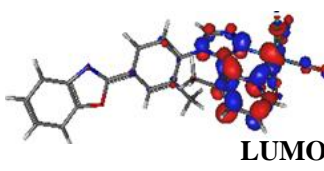
	RePBO-Me1	RePBO-Me2	RePBO-Me3
Spin density			
Hole	 HOMO	 HOMO	 HOMO-1
Particle	 LUMO	 LUMO	 LUMO

Figure S21. Representation of the three methylated complexes in the lowest MLCT triplet excited state, calculated by DFT at the PBE0/LANL2DZ level of theory. Spin density distribution (isovalue = 0.03 e bohr⁻³), position of unpaired electrons in the hole (HOMO or HOMO-1) and in the particle (LUMO). Data obtained from the comparison of the Kohn-Sham orbitals of the molecule in the triplet state with those of the ground state.

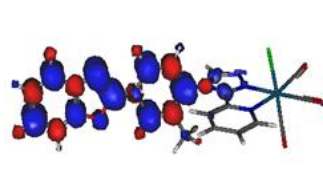
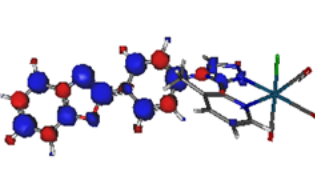
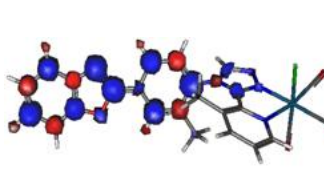
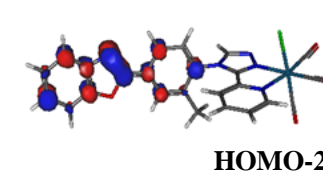
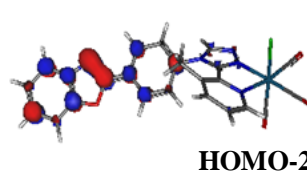
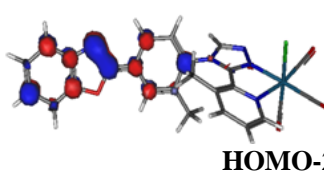
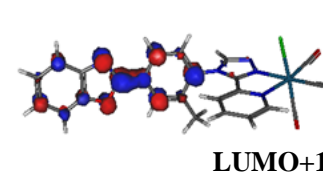
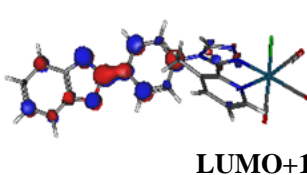
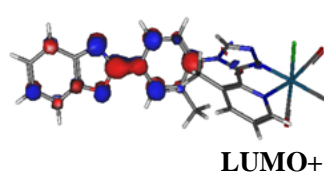
	RePBO-Me1	RePBO-Me2	RePBO-Me3
Spin density			
Hole	 HOMO-2	 HOMO-2	 HOMO-2
Particle	 LUMO+1	 LUMO+1	 LUMO+1

Figure S22. Representation of the three methylated complexes in the lowest ILCT triplet excited state, calculated by DFT at the PBE0/LANL2DZ level of theory. Spin density distribution (isovalue = 0.03 e bohr⁻³), position of unpaired electrons in the hole (HOMO-2) and in the particle (LUMO+1). Data obtained from the comparison of the Kohn-Sham orbitals of the molecule in the triplet state with those of the ground state.

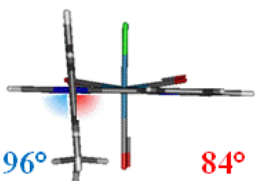
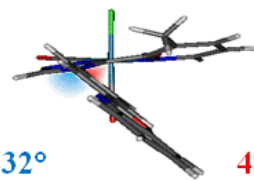
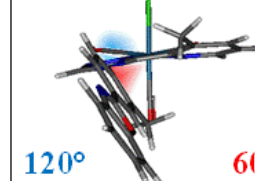
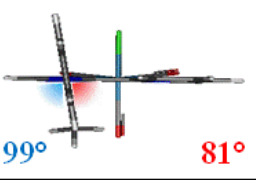
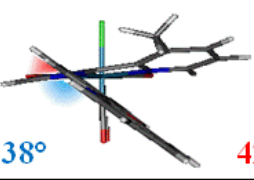
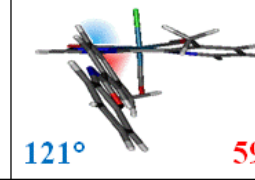
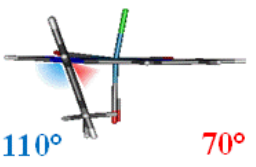
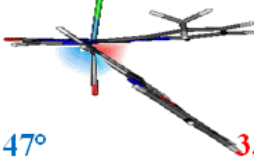
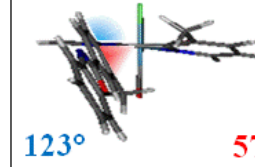
	RePBO-Me1	RePBO-Me2	RePBO-Me3
Ground state	 96° 84°	 132° 48°	 120° 60°
³ ILCT	 99° 81°	 138° 42°	 121° 59°
³ MLCT	 110° 70°	 147° 33°	 123° 57°

Figure S23. Geometry of the three methylated complexes in the ground state and in the two lowest excited triplet states ³ILCT and ³MLCT, calculated by using the DFT method at the PBE0/LANL2DZ level. The values of the phenyl-pyta angles obtained by calculations are indicated in blue ink. The complementary angles, taken for the crystallography discussion, are indicated in red ink.

Table S10. Comparison between the phenyl-pyta angle values (in °) determined by crystallography and calculated by DFT at the PBE0/LANL2DZ level of theory for molecules in the ground state and in the two lowest-energy triplet states. Between parentheses: value of the complementary angle estimated with respect to the right angle. Difference between the angles calculated for the molecule in the ground state and in the ³MLCT state (Δ (GS-³MLCT)).

Complex	Experimental (crystal)	Theoretical		
		Ground state	³ ILCT	³ MLCT
RePBO-Me1	73	96 (84)	99 (81)	110 (70)
RePBO-Me2	57	132 (48)	138 (42)	147 (33)
RePBO-Me3	63	120 (60)	121 (59)	123 (57)
RePBO	83.3 ^a	---	115 (65)	(55.5) ^a

^a: Data from Calupitan *et al.*, *Chem. Eur. J.* **2021**, *27*, 4191–4196.

Electrochemistry

Table S11. Selected electrochemical data of complexes **RePBO-Me1**, **RePBO-Me2** and **RePBO-Me3** (1.0×10^{-3} M). Values determined by OSWV on a Pt working electrode in $\text{CH}_2\text{Cl}_2 + 0.1$ M *n*- Bu_4NBF_4 at room temperature.^{a,b} Ferrocene was used as internal reference.

Compound	Oxidation		Reduction			
	E_2	E_1	E_1	E_2	E_3	E_4
RePBO-Me1	1.78	1.48	-1.28 ^c	-1.69 ^e	-1.86	
RePBO-Me2	1.74	1.46	-1.27 ^c	-1.56 ^f	-1.83	-1.95
RePBO-Me3	1.78	1.47	-1.28 ^c	-1.68 ^g	-1.77	-1.94
RePBO ^h	1.73	1.44	-1.28 ^c	-1.58	-1.83	
RePhe ⁱ	1.79	1.47	-1.31 ^d	---	---	

^a OSWVs were obtained using a sweep width of 20 mV, a frequency of 20 Hz, and a step potential of 5 mV.

^b Potential values in Volts vs. SCE (Fc^+/Fc is observed at $0.55 \text{ V} \pm 0.01 \text{ V vs. SCE}$).

^c One-electron quasi-reversible process at 0.2 V/s.

^d One-electron quasi-reversible process at 1 V/s.

^e Shoulder. In SW, until 1000/20/5, the two last reductions overlap and no real change is observed; idem in CV when changing the scan rate until 50 V/s.

^f in SW until 1000/20/5, no real change for the reduction waves; in CV the first reduction wave becomes reversible with increasing scan rate but the other three do not evolve and cannot be distinguished up to 50 V/s.

^g in SW until 1000/20/5, no real change. In CV, the first reduction wave becomes quasi-reversible with increasing scan rate, but the other three do not evolve and cannot be distinguished up to 10 V/s.

^h From, J. Wang *et al.*, *Dalton Trans.*, 2019, 48, 15906–15916.

ⁱ From, A. Poirot *et al.*, *Dalton Trans.*, 2021, 50, 13686–13698. **Re-Phe** = $[\text{Re}(\text{CO})_3(2-(4\text{-phenyl-4H-1,2,4-triazol-3-yl})\text{pyridine})\text{Cl}]$.

Table S12. Experimental electrochemical data used, and calculated values of the energy gaps (E_g) for complexes **RePBO-Me1**, **RePBO-Me2** and **RePBO-Me3**.

Compound	$E_{\text{onset ox}}$ (V)	$E_{\text{onset red}}$ (V)	E_{HOMO} (eV)	E_{LUMO} (eV)	E_g^{el} (eV)	$E_{\text{calc}}^{\text{a}}$ (eV)
RePBO-Me1	1.36	-1.16	-6.10	-3.58	2.52	2.94
RePBO-Me2	1.36	-1.15	-6.10	-3.59	2.51	2.93
RePBO-Me3	1.36	-1.18	-6.10	-3.56	2.54	2.95
RePBO	1.34	-1.16	-6.08	-3.58	2.50	2.65 ^b , 2.73 ^c

^a The values were obtained using the TD-DFT method and considering the optimized geometry of the S_1 state.

^b From, J. Wang *et al.*, *Dalton Trans.*, 2019, 48, 15906–15916

^c From, A. Poirot *et al.*, *Dalton Trans.*, 2021, 50, 13686–13698.

Evaluation of the energy gap values (E_g^{el}) for the Re complexes.

The onset oxidation and reduction potentials ($E_{\text{onset ox}}$, $E_{\text{onset red}}$) were measured by cyclic voltammetry in volt *versus* SCE. The CVs were carried out at a potential scan rate of 200 mV s^{-1} at room temperature.

The HOMO and LUMO energy levels (E_{HOMO} and E_{LUMO}) in electron volt (eV) were calculated according to the empirical equations (1) and (2):^[1]

$$E_{\text{HOMO}} (\text{eV}) = -e (E_{\text{onset ox}} (\text{V vs. SCE}) + 4.74 \text{ V}) \quad \text{Eq(1)}$$

$$E_{\text{LUMO}} (\text{eV}) = -e (E_{\text{onset red}} (\text{V vs. SCE}) + 4.74 \text{ V}) \quad \text{Eq(2)}$$

and the energy gap value was obtained as follows: $E_g^{\text{el}} = (E_{\text{LUMO}} - E_{\text{HOMO}})$.

The differences observed for the estimation of the energy gaps using experimental methods or theoretical calculations are well known. See for example: R. Stowasser, R. Hoffmann, *J. Am. Chem. Soc.* 1999, 121, 3414–3420.

[1] a) Y. Zhou, J. W. Kim, R. Nandhakumar, M. J. Kim, E. Cho, Y. S. Kim, Y. H. Jang, C. Lee, S. Han, K. M. Kim, J.-J. Kim and J. Yoon, *Chem. Commun.* 2010, 46, 6512–6514 and references therein; b) G. V. Loukova, *Chem. Phys. Lett.* 2002, 353, 244–252.

Electrochemical selected curves

OSWV study was performed on a Pt working electrode in $\text{CH}_2\text{Cl}_2 + 0.1 \text{ M } n[\text{Bu}_4\text{N}][\text{BF}_4]$ at room temperature in the presence of ferrocene used as internal reference. Frequency 20 Hz, amplitude 20 mV, step potential 5 mV. **Cyclic voltammograms** of the indicated compounds were performed on a Pt working electrode in $\text{CH}_2\text{Cl}_2 + 0.1 \text{ M } n[\text{Bu}_4\text{N}][\text{BF}_4]$ at room temperature at a scan rate of 0.2 V s^{-1} or at other mentioned scan rates.

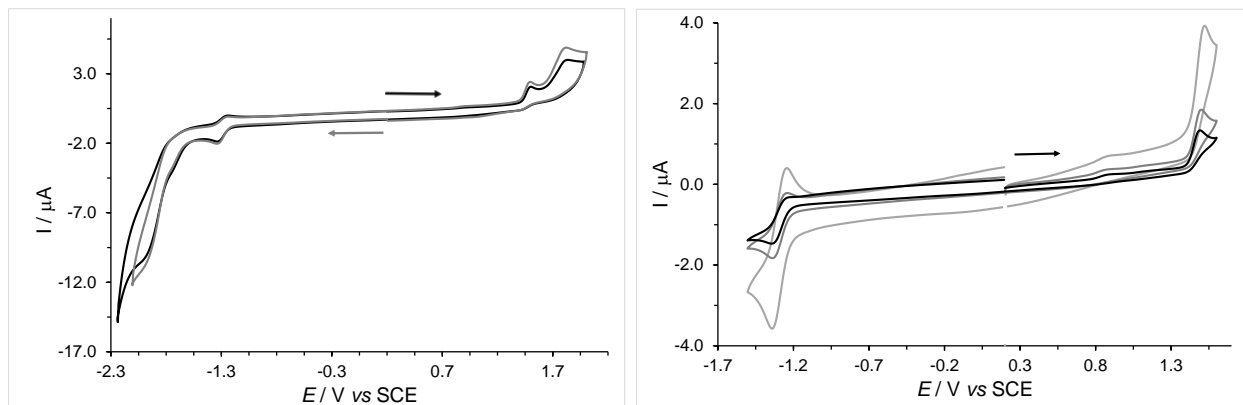


Figure S24. Cyclic voltammograms of complex **RePBO-Me1** (left), and of its first oxidation and reduction processes (right) at 0.1, 0.2 and 1.0 V/s.

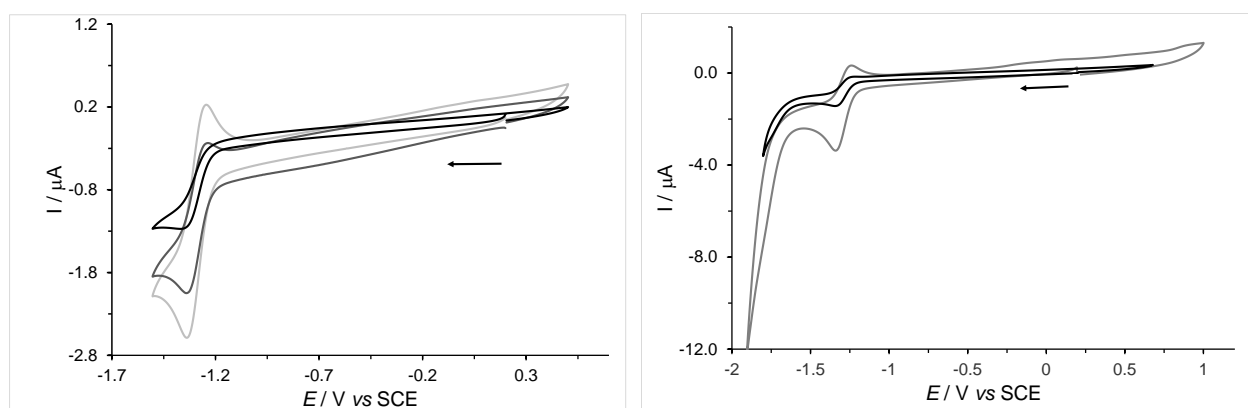


Figure S25. Cyclic voltammograms of the first reduction process of complex **RePBO-Me1** at 0.05, 0.2 and 0.5 V/s from bottom-black line to top-grey line (left), and of the reduction processes at 0.1 V/s black line, and 1.0 V/s grey line (right).

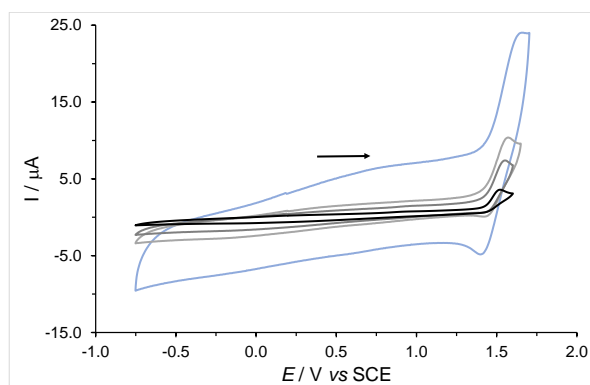


Figure S26. Cyclic voltammograms of the first oxidation process of complex **RePBO-Me1** at 1, 5, 10 and 50 V/s from bottom-black line to top-blue line.

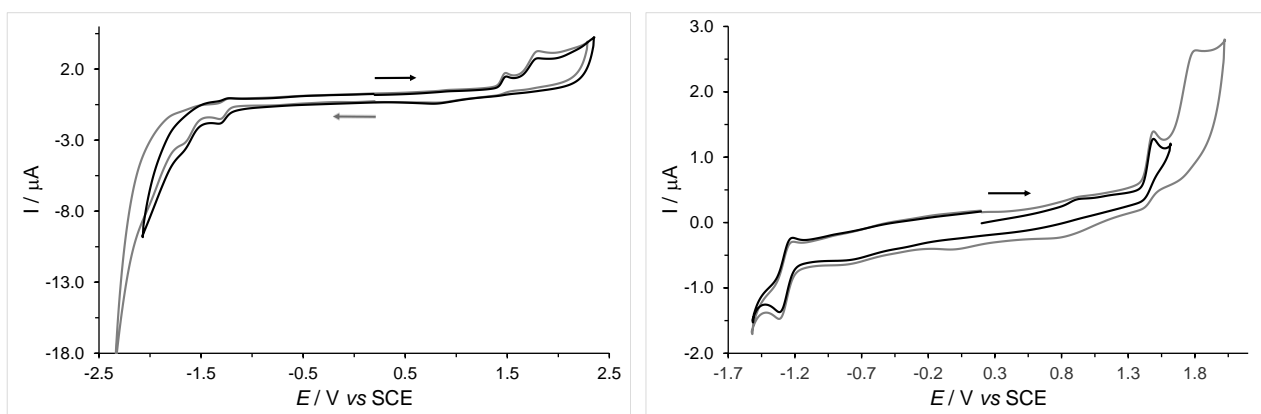


Figure S27. Cyclic voltammograms of complex **RePBO-Me2** (left), and of its first oxidation and reduction processes (right).

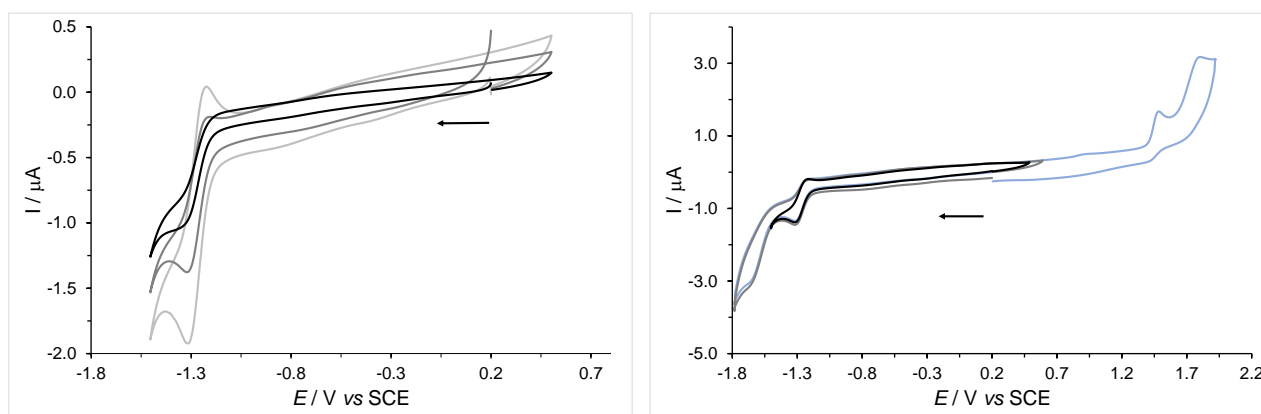


Figure S28. Cyclic voltammograms of the first reduction process of complex **RePBO-Me2** at 0.05, 0.2 and 0.5 V/s from bottom-black line to top-grey line (left), and of the compound at increasing potential (black, grey, blue) (right).

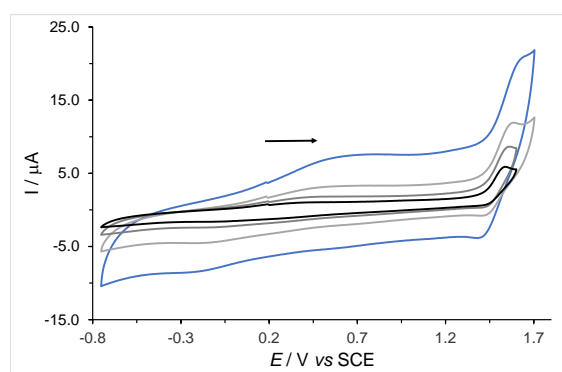


Figure S29. Cyclic voltammograms of the first oxidation process of complex **RePBO-Me2** at 5, 10, 20 and 50 V/s from bottom-black line to top-blue line.

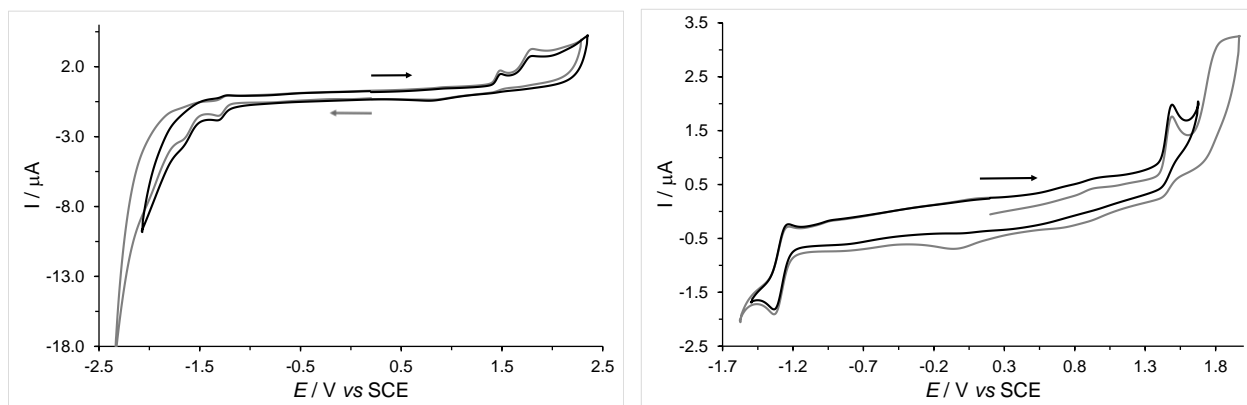


Figure S30. Cyclic voltammograms of complex **RePBO-Me3** (left), and of its first oxidation and reduction processes (right) at 0.1, 0.2 and 1.0 V/s.

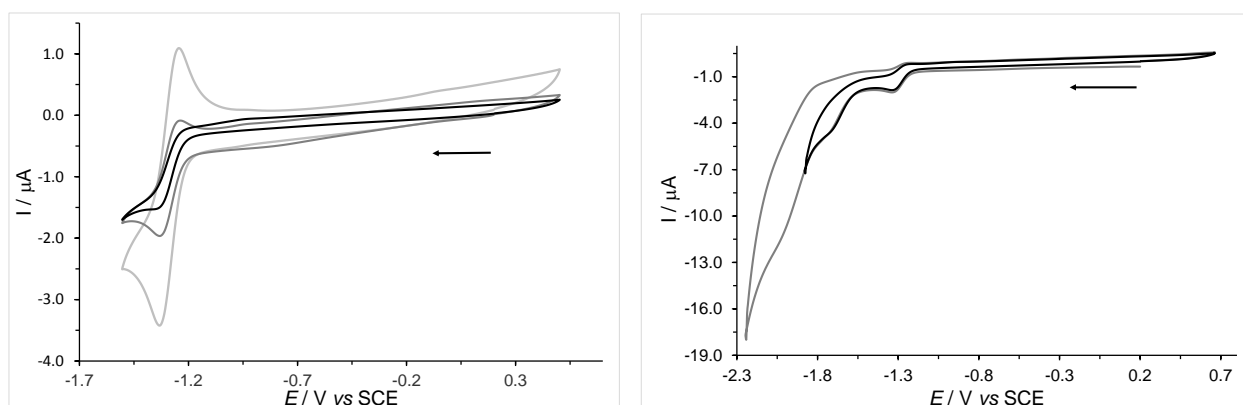


Figure S31. Cyclic voltammograms of the first reduction process of complex **RePBO-Me3** at 0.05, 0.2 and 0.5 V/s from bottom-black line to top-grey line (left), and of the compound at increasing potential in reduction (black, then grey).

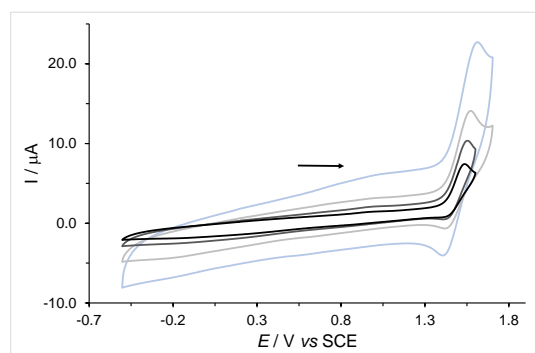


Figure S32. Cyclic voltammograms of the first oxidation process of complex **RePBO-Me3** at 5, 10, 20 and 50 V/s from bottom-black line to top-blue line

Spectroscopy

The fitted parameters are:

Hi reduced to: 2290 ch

SHIFT = 0.4138987 ch
1.721216E-10 sec
S.Dev = 6.783469E-12 sec

T1 = 167.9376 ch
6.98376E-08 sec
S.Dev = 7.454425E-11 sec

A = 26.68329
S.Dev = 0.1652849

B1 = 0.2445478
[100.00 Rel.Ampl]
S.Dev = 1.964135E-04

CHISQ = 1.387407
[2286 degrees of freedom]

Chi-squared Probability = 1.9288E-20%
Durbin-Watson Parameter = 1.539427
Negative residuals = 47.07423%
Residuals < 1 s.dev = 63.49345%
Residuals < 2 s.dev = 93.49345%
Residuals < 3 s.dev = 98.64629%
Residuals < 4 s.dev = 99.47598%

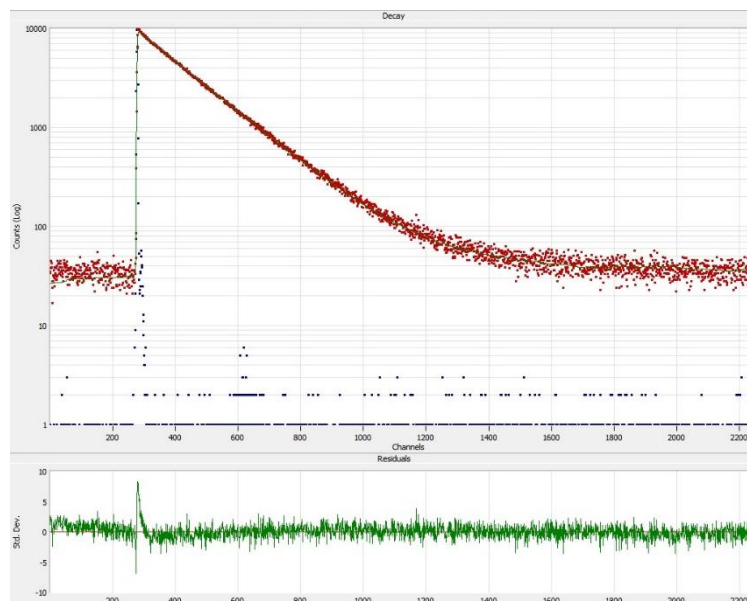


Figure S33. Photoluminescence decay of **RePBO-Me1** ($\sim 1.2 \times 10^{-5}$ M) in dichloromethane. $\lambda_{\text{ex}} = 371$ nm, $\lambda_{\text{em}} = 626$ nm.

The fitted parameters are:

Hi reduced to: 2190 ch

SHIFT = 0.2448283 ch
1.018129E-10 sec
S.Dev = 7.286076E-12 sec

T1 = 130.3608 ch
5.421112E-08 sec
S.Dev = 6.968784E-11 sec

A = 49.6722
S.Dev = 0.1959465

B1 = 0.2459051
[100.00 Rel.Ampl]
S.Dev = 2.246146E-04

CHISQ = 1.406187
[2186 degrees of freedom]

Chi-squared Probability = 1.9288E-20%
Durbin-Watson Parameter = 1.446519
Negative residuals = 45.6621%
Residuals < 1 s.dev = 64.20091%
Residuals < 2 s.dev = 92.51141%
Residuals < 3 s.dev = 98.94977%
Residuals < 4 s.dev = 99.45206%

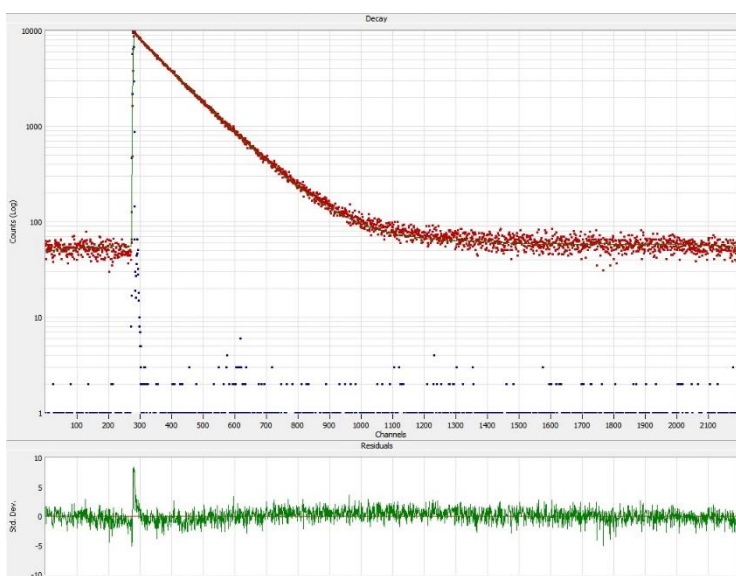


Figure S34. Photoluminescence decay of **RePBO-Me2** ($\sim 1.2 \times 10^{-5}$ M) in dichloromethane. $\lambda_{\text{ex}} = 371$ nm, $\lambda_{\text{em}} = 640$ nm.

The fitted parameters are:

Hi reduced to: 540 ch

SHIFT = 0.5393141 ch
8.971047E-10 sec
S.Dev = 2.211131E-11 sec

T1 = 37.40254 ch
6.221605E-08 sec
S.Dev = 2.244618E-10 sec

A = 263.7278
S.Dev = 0.8412696

B1 = 0.9980803
[100.00 Rel.Ampl]
S.Dev = 1.832231E-03

CHISQ = 2.277248
[536 degrees of freedom]

Chi-squared Probability = 1.9288E-20%

Durbin-Watson Parameter = 2.204093

Negative residuals = 48.51852%

Residuals < 1 s.dev = 66.11111%

Residuals < 2 s.dev = 93.33334%

Residuals < 3 s.dev = 98.51852%

Residuals < 4 s.dev = 99.25926%

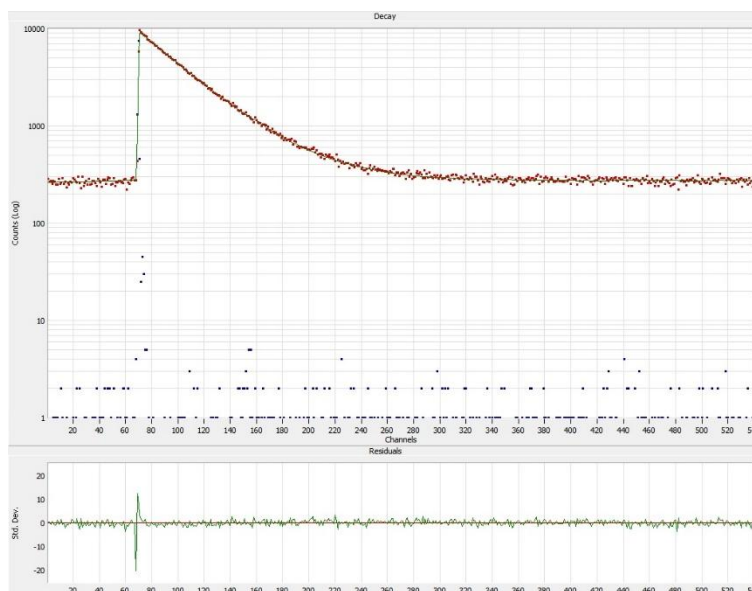


Figure S35. Photoluminescence decay of **RePBO-Me3** ($\sim 1.2 \times 10^{-5}$ M) in dichloromethane. $\lambda_{\text{ex}} = 371$ nm, $\lambda_{\text{em}} = 634$ nm.

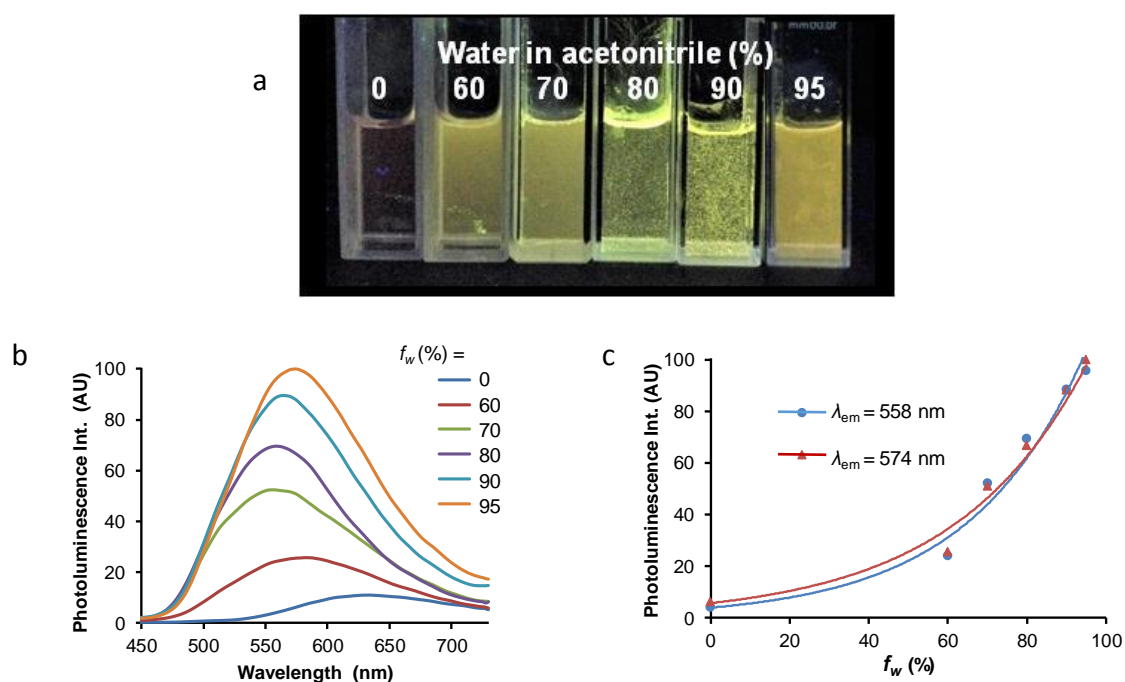


Figure S36. AIE behavior of **RePBO**. a) Samples of **RePBO** (3.6×10^{-5} M) in acetonitrile solutions containing 0, 60, 70, 80, 90, and 95% water, illuminated by UV light (365 nm). b) Corresponding emission spectra, $\lambda_{\text{ex}} = 380$ nm. c) Evolution of the photoluminescence intensity at 558 and 574 nm vs the water fraction f_w . Images (a) and (b) from Wang *et al.*, *Dalton Trans.* **2019**, 48, 15906–15916.

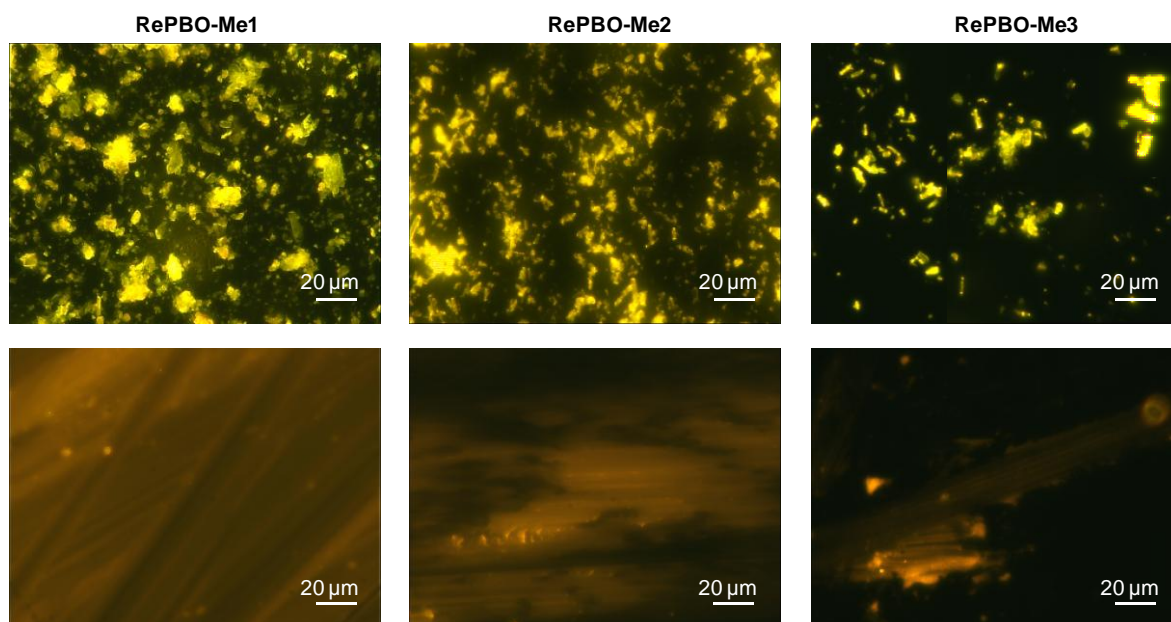


Figure S37. Fluorescence microscopy images of the three methylated complexes as pristine powders (top) and after grinding with a spatula (bottom).

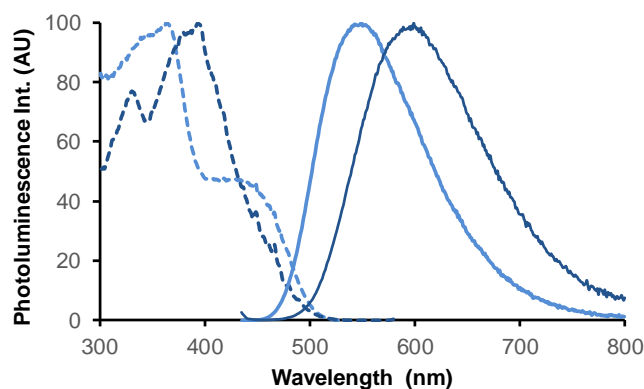


Figure S38. Photoluminescence excitation (dotted lines) and emission (full lines) spectra of **RePBO-Me1** as pristine (light blue) and ground (dark blue) powders. For excitation spectra: $\lambda_{em} = 549$ nm and 597 nm for pristine and ground powders, respectively. For emission: $\lambda_{ex} = 420$ nm for both samples.

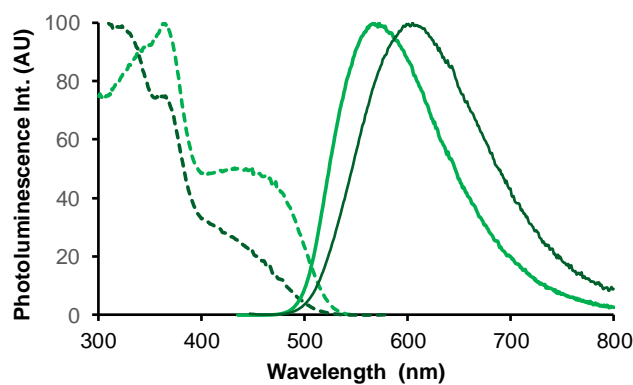


Figure S39. Photoluminescence excitation (dotted lines) and emission (full lines) spectra of **RePBO-Me2** as pristine (light green) and ground (dark green) powders. For excitation spectra: $\lambda_{em} = 570$ nm and 605 nm for pristine and ground powders, respectively. For emission: $\lambda_{ex} = 420$ nm for both samples.

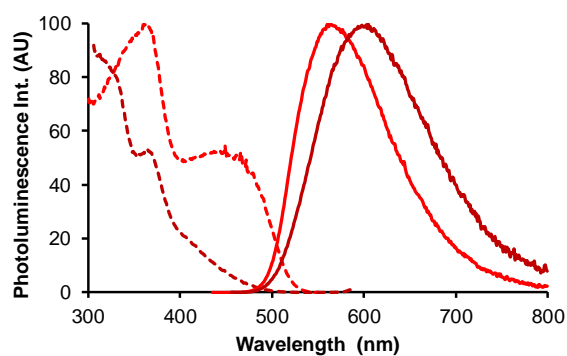


Figure S40. Photoluminescence excitation (dotted lines) and emission (full lines) spectra of **RePBO-Me3** as pristine (light red) and ground (dark red) powders. For excitation spectra: $\lambda_{em} = 563$ nm and 600 nm for pristine and ground powders, respectively. For emission: $\lambda_{ex} = 420$ nm for both samples.

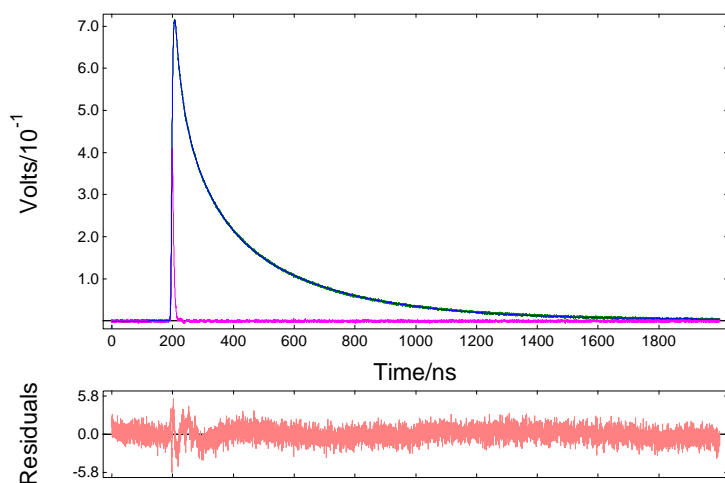


Figure S41. Photoluminescence decay of **RePBO-Me1** as pristine powder. $\lambda_{ex} = 420$ nm, $\lambda_{em} = 550$ nm.

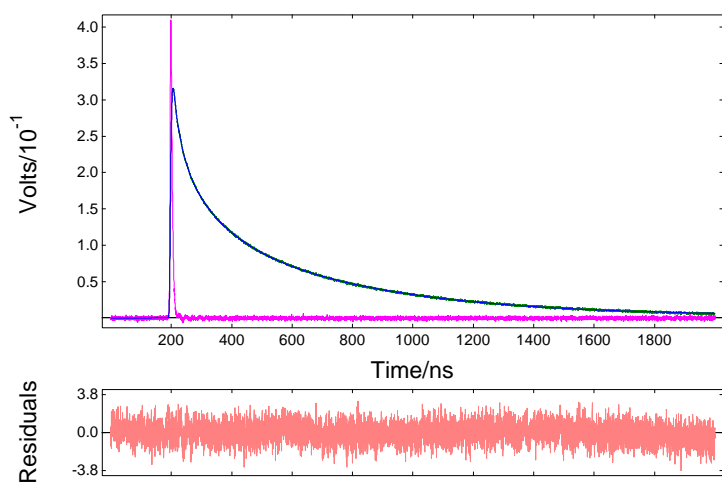


Figure S42. Photoluminescence decay of **RePBO-Me2** as pristine powder. $\lambda_{ex} = 420$ nm, $\lambda_{em} = 570$ nm.

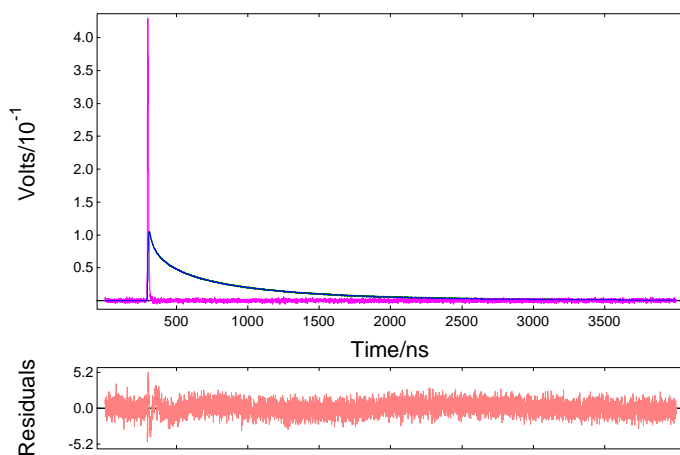


Figure S43. Photoluminescence decay of **RePBO-Me3** as pristine powder. $\lambda_{\text{ex}} = 420$ nm, $\lambda_{\text{em}} = 565$ nm.

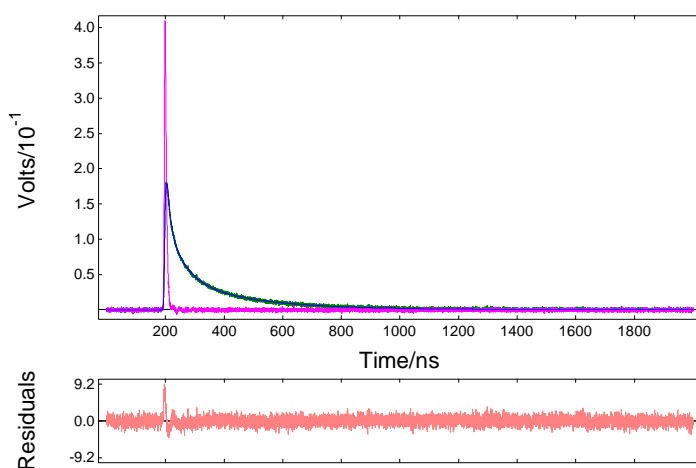


Figure S44. Photoluminescence decay of **RePBO-Me1** as ground powder. $\lambda_{\text{ex}} = 420$ nm, $\lambda_{\text{em}} = 600$ nm.

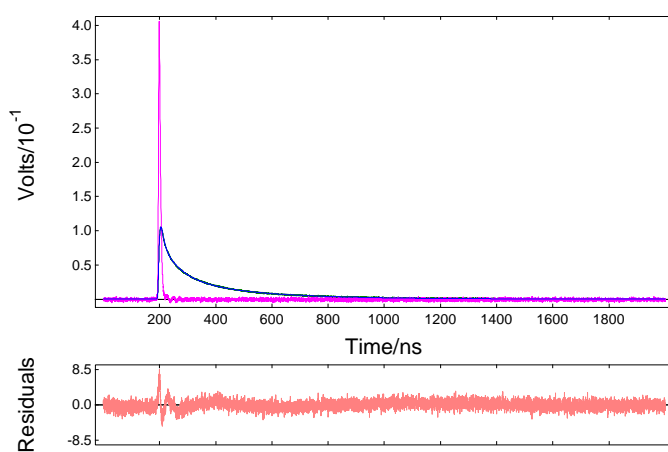


Figure S45. Photoluminescence decay of **RePBO-Me2** as ground powder. $\lambda_{\text{ex}} = 420$ nm, $\lambda_{\text{em}} = 605$ nm.

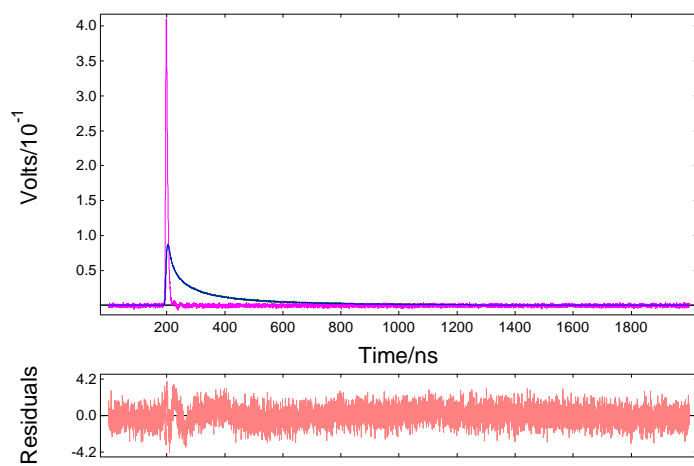


Figure S46. Photoluminescence decay of **RePBO-Me3** as ground powder. $\lambda_{\text{ex}} = 420 \text{ nm}$, $\lambda_{\text{em}} = 600 \text{ nm}$.